NASA TECHNICAL NOTE

NASA TN D-6556

RESPONSE OF A RADIAL-BLADED CENTRIFUGAL PUMP TO SINUSOIDAL DISTURBANCES FOR NONCAVITATING FLOW

by Douglas A. Anderson, Robert J. Blade, and William Stevans

Lewis Research Center
Cleveland, Ohio 44135

NATIONAL AERONAUTICS AND SPACE ADMINISTRATION • WASHINGTON, D. C. • DECEMBER 1971

1. Report No.	2. Government Accession No.	3. Recipient's Catalog No.
NASA TN D-6556		

4. Title and Subtitle	5. Report Date
RESPONSE OF A RADIAL-BLADED CENTRIFUGAL PUMP TO SINUSOIDAL DISTURBANCES FOR NONCAVITATING FLOW	December 1971
	6. Performing Organization Code

7. Author(s)	8. Performing Organization Report No.
Douglas A. Anderson, Robert J. Blade, and William Stevans	E-5877
	10. Work Unit No. 128-31
9. Performing Organization Name and Address Lewis Research Center National Aeronautics and Space Administration Cleveland, Ohio 44135	11. Contract or Grant No.
	13. Type of Report and Period Covered Technical Note
12. Sponsoring Agency Name and Address National Aeronautics and Space Administration Washington, D. C. 20546	14. Sponsoring Agency Code

15. Supplementary Notes

16. Abstract

A radial-bladed centrifugal pump was run in water with sinusoidal fluctuations of pressure and flow rate imposed at the pump inlet. Since the flow was noncavitating, zero gain was assumed in computing pump impedance. The inertive reactance became greater than the resistance at relatively low frequencies. An electric circuit model was developed in order to explain the trends of inertance and resistance with frequency.

17. Key Words (Suggested by Author(s))	18. Distribution Statement
Pogo Dynamics Pumps Hydraulics Pump dynamics	Unclassified - unlimited

19. Security Classif. (of this report)	20. Security Classif. (of this page)	21. No. of Pages	22. Price*
Unclassified	Unclassified	52	$3.00

* For sale by the National Technical Information Service, Springfield, Virginia 22151

CONTENTS

RESPONSE OF A RADIAL-BLADED CENTRIFUGAL PUMP TO SINUSOIDAL DISTURBANCES FOR NONCAVITATING FLOW

by Douglas A. Anderson, Robert J. Blade, and William Stevans

Lewis Research Center

SUMMARY

A radial-bladed centrifugal pump was run in water with sinusoidal fluctuations of pressure and flow rate imposed at the pump inlet. The pump response was determined by measurements of appropriate fluctuating pressures and flow rates. Since the flow was noncavitating, zero gain was assumed in computing pump impedance. Furthermore, it was shown that the gain computed from the data was zero within the accuracy of the measurements.

The pump impedance was found to be a complex value composed of resistance and inertive reactance. The reactance was greater than the resistance except at relatively low frequencies (below 3 to 9 Hz, depending on the flow rate). The resistances computed from the steady-state performance curves agreed reasonably well with the dynamic values at zero frequency. Both resistance and inertance were frequency dependent, with the greatest changes occurring below 20 hertz. For the impeller-volute combination, the resistance increased with frequency while the inertance decreased. For the outlet diffuser, the resistance and inertance were almost independent of frequency near design flow, but had significant low-frequency trends at higher flows. The high-frequency diffuser inertance agreed with the value computed from the diffuser geometry.

An electric circuit model was developed in order to explain the trends of impedance with frequency. The model does not require any dynamic measurements. The model results agreed reasonably well with the measured data near design flow and at high frequencies for higher than design flows. However, the model does not explain some of the low-frequency-data trends at the higher flows. These trends are probably due to the effects of the uneven flow distribution in the impeller and the volute.

INTRODUCTION

In launch vehicles, the longitudinal structural oscillations often referred to as

"pogo" are a serious problem. These oscillations result from the coupling of the vehicle structure and the vehicle propulsion system in a closed-loop feedback arrangement. To analyze these oscillations requires that each component of the closed loop be represented by an appropriate transfer function. One of the problems encountered in pogo studies is in predicting with sufficient accuracy the response of the propellant pumps to variations in inlet pressure and flow rate.

The pump is commonly represented in terms of gain and impedance as is explained in reference 1. While gain and impedance can be related to the steady-state operating characteristics of the pump, reference 1 indicates that it is preferable to base the representation on dynamic data. Two attempts to determine pump dynamic response experimentally are reported in references 2 and 3. Reference 2 presents some dynamic measurements made in liquid oxygen and liquid hydrogen, and suggests a different representation of the pump than reference 1. Reference 3 gives some results in which the input perturbations were created by shaking the pump.

In the investigations to date, the analysis of cavitating dynamic data requires some prior assumptions to be made about pump impedance or gain. An experimental investigation was carried out at the NASA Lewis Research Center in order to obtain more complete dynamic data. One of the purposes of this investigation was to allow the determination of unambiguous values of pump gain and impedance. Reference 4 describes the test facility used in this investigation and the design philosophy on which it is based.

Some work was also done to define the trends of noncavitating pump impedance with frequency. This is the main concern of the present report. Data are presented which were taken at noncavitating inlet pressures over a range of frequencies and flow rates. For noncavitating flow, the dynamic equations become less complicated since gain is zero. This allows the pump impedance to be calculated in a more straightforward manner, and makes the results less sensitive to measurement errors.

TEST FACILITY AND INSTRUMENTATION

The test facility used in this investigation is a closed-loop water tunnel. Only a brief description of the test facility and instrumentation will be given herein, as a detailed description appears in reference 4. The test facility has subsystems which are used to generate and measure sinusoidal perturbations of pressure and flow rate. A schematic diagram of the test facility is shown in figure 1(a), and a photograph in figure 2.

Test Pump

The pump selected for these tests has an unshrouded radial-bladed centrifugal impeller and a single discharge volute. A sketch of the pump internal geometry is shown in figure 1(b), and a photograph of the impeller in figure 3. The complete steady-state performance of the pump impeller is given in reference 5.

Flow and Pressure Perturbing System

The purpose of this system is to generate small sinusoidal flow and pressure pulsations at the pump inlet. The system is located between the inlet isolation tank and the inlet line. One component of the system is a perturbation throttle designed especially for the test facility. A precisely controlled variation in throttle flow area produces the desired flow and pressure fluctuations.

Dynamic Pressure Measurements

These measurements were made with flush-diaphragm, strain-gage pressure sensors. These sensors are placed at 10 locations, labeled 1 to 10 in figure 1(a). The electrical signals from the sensors were measured in phasor form by using a transfer function analyzer. Phase data were obtained by comparing the signal to be measured to a reference signal (the same signal as was used to drive the perturbation throttle).

Inlet Dynamic Flow Measurement

The perturbed flow approaching the pump was computed from the pressure measurements on the inlet line (stations 1 to 5 of fig. 1(a)). The perturbed flow rate is related to these pressures by the acoustical wave equation as given in reference 4 (eq. (1)).

Vibration Measurement

The longitudinal motion of the inlet line near the pump was measured with two different motion sensors. This motion is taken into account in the calculation of the perturbed flow into the pump. Reference 4 showed that if the vibration correction were neglected, gross errors would result.

Outlet Dynamic Flow Measurement

The perturbed flow leaving the pump was determined by measuring the perturbed pressure drop across a specially designed multihole orifice plate. Figure 1(a) shows the location of the orifice plate and of the pressure sensors (labeled 9 and 10). The orifice plate is shown in figure 4. The purpose of the special design is to minimize the inertive component of the orifice plate dynamic impedance, as discussed in reference 4.

Open Orifice and Blocked Orifice

One of the requirements of the test program was that data be taken at two different system exit impedances. The two impedances were obtained by using two different outlet orifice configurations, referred to as the open orifice and the blocked orifice. Open orifice denotes the multihole orifice plate as originally fabricated. Blocked orifice denotes the same orifice plate with 20 percent of the holes filled with epoxy plastic. The blocked orifice had a dynamic resistance 63 percent higher than the open orifice.

Steady-State Measurements

Steady-state pressure measurements were made with strain-gage pressure sensors. Measurements were made of pump inlet and outlet total pressure, and of wall static pressures at stations 6, 8, 9, and 10 of figure 1(a). Steady-state flow rate was measured by using a venturi and a bi-fluid manometer. The rotational speed of the pump was measured by using a magnetic pickup.

APPROACH

Pump dynamic response is generally described in terms of gain, impedance, and compliance. This report is concerned primarily with the experimental determination of pump impedance. The following discussion first presents the method developed in reference 4 for determining impedance and gain. After that, the simplifications possible for the case of noncavitating flow are discussed. These simplifications are of special interest in this report, which analyzes only noncavitating data.

The standard equation used to represent pump dynamic response is (ref. 1)

$$P_D = (m + 1)P_S - ZQ_{out} \tag{1}$$

Equation (1) is a phasor equation in which P_D refers to the perturbed discharge total pressure, P_S the perturbed suction total pressure, and Q_{out} the perturbed outlet flow rate. (All symbols are defined in appendix A. Throughout this report, pressures and flow rates are perturbed parameters unless otherwise stated.) This equation is based on the assumption that the perturbed flow is equal to Q_{out} everywhere within the pump. Any compliance due to cavitation or to pump structural flexibility is assumed to act at the pump inlet but not within the pump itself. In using equation (1), the values of P_D, P_S, and Q_{out} are obtained from the test data of this investigation. Pump gain m and pump impedance Z are then to be calculated from these values.

In general, the values of m and Z cannot be determined from a single set of P_D, P_S, and Q_{out} values. There are two unknowns but only one equation. In the method of reference 4, two sets of data are taken at the same steady-state conditions but with different exit impedances in the test loop. Changing the exit impedance changes the ratios of P_D/Q_{out} and P_S/Q_{out} without changing the pump gain m or the pump impedance Z. Thus, the two sets of data provide two equations from which the two unknowns m and Z can be determined. In the test facility, two different exit impedances were obtained by using two different configurations of the multihole orifice plate.

The gain m accounts for the effect of cavitation on the pump response to pressure perturbations. For steady-state operation, gain is equal to the slope of the pump head rise plotted against inlet head. For dynamic operation, gain will, in general, be a complex number. For noncavitating flow, gain should theoretically be zero. All the data shown in this report are noncavitating, and the zero-gain assumption was used in calculating impedance. The significance of the gain data is examined in the section RESULTS AND DISCUSSION and in appendix C. It was confirmed that gain is zero within the measurement accuracy of the data.

Assuming that the gain is zero, a value of pump impedance can be computed from a single set of data. Denoting this value as Z_{nc},

$$Z_{nc} = \frac{P_S - P_D}{Q_{out}} \tag{2}$$

The impedance will generally be a complex number.

Two sets of noncavitating data were taken using two different multihole orifice plate configurations. The two sets are referred to as the open-orifice data and the blocked-orifice data. The pump impedance can be computed from both sets of data by using equation (2); comparing the results then gives an indication of data consistency. The pump impedance can also be computed by a simultaneous solution using equation (1). However, for the test data obtained in this investigation, the effect of measurement

errors was magnified when the simultaneous solution was used. Consequently, the most accurate values of impedance are those computed by using equation (2).

DATA REDUCTION

Perturbed-Flow-Rate and Total-Pressure Calculation

The outlet perturbed flow rate is computed by using the following equation, which is a rearranged form of equation (9) of reference 4:

$$Q_{out} = \frac{p_9 - p_{10}}{R_{or} + j2\pi f L_{9-10}} \tag{3}$$

where $p_9 - p_{10}$ is the perturbed pressure difference measured across the orifice plate, R_{or} is the resistance of the orifice plate, and L is the inertance of the pipe between the two measuring stations. The resistance R_{or} is determined from the steady-state orifice calibration curve. Perturbed total pressures are computed from

$$P = p + \frac{\rho}{A^2} Q_{av} Q \tag{4}$$

where A is the cross-sectional area of the pipe at the pressure measuring station, and Q_{av} is the steady-state flow rate. In equations (3) and (4), the basic measured quantities are the perturbed static pressures p.

Impedance Calculation

The pump impedance was computed from the perturbed total pressures and the perturbed outlet flow rate by using equation (2). This method is correct only for noncavitating data. The impedance is expected to be a complex number, with the imaginary part due to inertance. Thus, impedance can be written in the form

$$Z_{6-8} = \frac{P_6 - P_8}{Q_{out}} = R_{6-8} + jX_{6-8} = R_{6-8} + j2\pi f L_{6-8} \tag{5}$$

where Z denotes impedance, R resistance, X reactance, and L inertance. The

symbols P and Q refer to perturbed pressure and flow rate. Total pressures are used in the calculation as it is shown in appendix B that this is the correct choice for the general case of nonzero mean flow. The subscripts 6 and 8 refer to the measurement locations as shown in figure 1(b), and Z_{6-8} refers to the impedance between these two stations. Z_{6-8} is the combined impedance of the impeller and the volute. Two other impedances, Z_{8-9} and Z_{6-9} are also used; they are defined similarly. Z_{8-9} is the impedance of the conical diffuser, and Z_{6-9} is the impedance of the whole pump.

Gain Calculation

In the method of reference 4, pump gain is computed from two sets of data (the open-orifice data and the blocked-orifice data) taken at the same steady-state conditions but with different exit impedances in the test system. For the open orifice, equation (1) becomes

$$P_{D,O} = (m + 1)P_{S,O} - ZQ_O \tag{6}$$

(The subscript out has been omitted from Q_{out}. There is no chance of confusion, since only outlet flows appear in the equations.) For the blocked orifice,

$$P_{D,B} = (m + 1)P_{S,B} - ZQ_B \tag{7}$$

The pump gain m is assumed to be the same in both equations, so is the pump impedance Z. Solving the two equations for gain,

$$m + 1 = \frac{P_{D,O}Q_B - P_{D,B}Q_O}{P_{S,O}Q_B - P_{S,B}Q_O} \tag{8}$$

This equation gives gain entirely in terms of measured quantities.

RESULTS AND DISCUSSION

All the data shown in this report were taken at the noncavitating inlet pressure of 4.83×10^5 newtons per square meter gage (70 psig). (In ref. 5, the first effects of cavitation on performance were observed at an inlet pressure of approximately 3.79×10^5 N/m^2 gage (55 psig).) In order to study the effect of frequency on the pump dynamic

performance, data were taken at selected frequencies ranging from 2 to 52 hertz. The effect of flow rate was also investigated; the dynamic performance data were taken at three steady-state flow coefficients (0.442, 0.497, and 0.536) in the high-flow part of the pump operating range. Changes in flow rate result in changes in the impeller steady-state flow distribution, as discussed in reference 5. At higher flows, the flow rate through the impeller passage in front of the volute tongue is considerably higher than through the passages behind the tongue. Near the design flow coefficient of 0.363, there is approximately equal flow through all the passages. Some of the trends in the dynamic response of the pump can be explained to be the result of the changes in the steady-state flow distributions.

Steady-State Performance

The steady-state performance of the pump is shown in figure 5. Figure 5(a) shows the combined performance of the impeller and the volute, as measured just upstream of the conical diffuser. Figure 5(b) shows the performance of the complete pump (measured at the diffuser outlet), and figure 5(c) the performance of the conical diffuser. It would be more conventional to show the diffuser performance in terms of a loss coefficient; however, the head rise coefficient is used so that figure 5(c) conforms to the other two figures. The steady-state curves are of interest in dynamic studies since theoretically as the frequency approaches zero, the resistances should approach the slopes of the curves expressed in appropriate units (N-sec/m^5, or lbf-sec/ft^5). The steady-state pressure measurements were made at the same measurement stations (6, 8, and 9 of fig. 1(b)) as the dynamic measurements. Total pressure was measured directly at measurement station 6, but only static pressures were measured at stations 8 and 9. The total pressures at the latter stations were obtained by adding the velocity head, using a velocity computed by dividing the overall flow rate by the flow area at the respective measurement station. The measured pressures at stations 6 and 8 agreed closely with those of reference 5 (in ref. 5, measurement station 8 is designated 5c). This comparison can not be made for station 9, which was not included in the reference 5 measurements.

There are some discrepancies in the open-orifice data. Four of the open-orifice data points of figure 5(b), taken on one day, agree with the blocked-orifice data. Three of the open-orifice data points, all taken on another particular day, are all low. Unfortunately, the pressure at measurement station 8 was not recorded for the four good data points, so only the three questionable data points appear in figures 5(a) and (c).

Perturbed Flow Rates and Total Pressures

The magnitudes of the perturbed pressures and flow rates are shown in figure 6 for a typical run. The greatest perturbed flow rate was about 4 percent of the steady-state flow rate (0.0388 m^3/sec, or 1.37 ft^3/sec). The peaks at 17 hertz are due to changes in the acoustic impedance of the inlet line. Above 30 hertz the data are greatly affected by the longitudinal vibration of the inlet line, which had a resonant frequency of 34 hertz. This vibration is the cause of the differences between the flow out of the inlet line Q_5 and the flow into the pump Q_{in}. The result is a low magnitude of Q_{in} which, in turn, affects all the pump perturbed pressures and flow rates. The impedance data (figs. 7 to 10) are computed from ratios of the measured pressures and flows. Thus, the ups and downs of figure 6 do not appear in the impedance data. There is, however, an indirect effect. The measurement accuracy is poor when the measured quantities get too small. This explains the increase in the scatter of the impedance data which occurs in the frequency range of 30 to 40 hertz.

Some analysis of the perturbed pressure and flow data was done in reference 4. Several checks were made on the consistancy of the perturbed flow measurements. The amount of data scatter in the compliance flow suggested an accuracy of no worse than 2 percent in the inlet and outlet flow values. The noncavitating pump compliance was found to be large enough to cause significant differences to occur between the inlet and outlet perturbed flows. (A compliance value of 2.66×10^{-11} m^5/N (4.5×10^{-8} ft^5/lbf) was determined from the dynamic data.) Compliance is not a major concern in the present report, since all the results shown are based on the outlet perturbed flow. However, a complete representation of the pump dynamic response would have to include a compliance term to give the relation between inlet perturbed flow and outlet perturbed flow.

Pump Impedance

Three different impedances were computed; they are identified by their subscripts. Z_{6-8} denotes the combined impedance of the impeller and the volute, Z_{8-9} the impedance of the diffuser, and Z_{6-9} the impedance of the whole pump. The impedance values were computed by using equation (2). Since this equation was derived assuming zero gain, it is valid only for noncavitating flow

Impedance data. - The general trends of impedance with frequency are depicted in figure 7. The impedances Z_{6-8} and Z_{6-9} are shown for the open-orifice data at two flow coefficients (0.442 and 0.536). (The blocked-orifice data have the same general trends as the open-orifice data.) The impedances are presented in terms of their real parts (resistance R) and their imaginary parts (reactance X). All the reactances shown

are approximately directly proportional to frequency. This shows that they are caused by inertance, as anticipated. (Inertance is a parameter in hydraulic systems analogous to electrical inductance.) A significant point is the relatively low frequency at which reactance becomes important. In fact, the reactance X_{6-9} becomes as large as the resistance R_{6-9} at approximately 9 hertz at the high flow and 3 hertz at the low flow.

In figures 8 to 10, the data are shown in terms of resistance and inertance. While figure 7 gives a better picture of the trends of pump response with frequency, figures 8 to 10 are easier to analyze. This is because inertance is a convenient parameter to use in the electrical circuit analogy of a hydraulic system. All the noncavitating dynamic performance data are presented in figures 8 to 10, both the open-orifice and blocked-orifice data at all three flow coefficients. The dynamic representation of the whole pump, which is the item of interest in pogo studies, is given by R_{6-9} and L_{6-9} of figures 8(a) and (b), respectively. But in explaining the results, it is necessary to look at the separate contributions of the impeller-volute combination (R_{6-8} and L_{6-8} of figs. 9(a) and (b), respectively) and of the conical diffuser (R_{8-9} and L_{8-9} of figs. 10(a) and (b)).

Data consistency. - One indication of data consistency is how well the impedance data of figures 8 to 10 agree for the two different outlet orifice configurations. The two configurations are identified as the blocked orifice and the open orifice. Theoretically, the data of figures 8 to 10 should not be affected by a change in outlet impedance, because gain is assumed to be zero. The differences appearing in the figures should therefore be due to measurement errors and errors in setting the operating point (the same steady-state conditions could not be duplicated exactly for two different runs).

In all the figures, there is good agreement between the open-orifice data and the blocked-orifice data. For most of the figures, no differences other than data scatter can be seen. However, for the inertance plots (figs. 8(b), 9(b), and 10(b)) at a pump flow coefficient $\overline{\varphi}$ of 0.497, there is a systematic difference between the two types of data of about 7 percent. The same percentage difference occurs in all three plots. This result, if it is due to measurement errors, would be caused by an error in Q_{out} rather than by an error in one of the pressures p_6, p_8, or p_9. An error in one of the pressures would affect only two of the three plots. The explanation of an error in Q_{out} could be either an error in the measurement of the perturbed pressure across the outlet orifice plate, or an error in the steady-state flow measurement. (The latter would give an incorrect value of the resistance R_{or} appearing in eq. (3).)

A few tests were run with a vibration absorber added to the system to reduce the vibration of the inlet line. The results of these tests are shown as tailed data points in figures 8 to 10. There is no significant difference from the rest of the data. This indicates, as discussed in reference 4, that the effect of inlet line vibrations was correctly accounted for in the method used for reducing the data.

Impedance is a complex number, and its computed value will have an error in magnitude and an error in phase angle. At high frequencies, the reactive part of the impedance is much greater than the resistive part; consequently, an error in phase angle gives a comparatively large error in resistance. At low frequencies the opposite is true; so an error in phase angle gives a large error in inertance. In these cases, the individual resistance or inertance plot may show an increase in data scatter which does not indicate poorer measurement accuracy.

Steady-state resistance values. - Theoretically, the resistance values at zero frequency can be calculated from the slopes of the steady-state head-flow curves. When dynamic data are not available, these steady-state resistance values can be used in an approximate analysis of the transient response of a pump. The steady-state resistance values were computed from the curves of figure 5. Because other curves could be drawn which appear to fit the data points equally well but have considerably different slopes, these resistance values are not expected to be very accurate. The slope of a performance curve will not be well defined unless the data points are closely spaced and unusually accurate. The steady-state resistance values are shown on figures 8(a), 9(a), and 10(a) by the symbol R_{SS}. The agreement with the dynamic resistance values extrapolated to zero frequency is probably within the accuracy to which R_{SS} can be determined.

Resistance and inertance trends with frequency. - Figure 9 shows that as frequency is increased, R_{6-8} increases while L_{6-8} decreases. The greatest changes occur at low frequencies; above roughly 20 hertz, changes are small.

These trends can be explained by considering the effect of inertance on the pattern of perturbed flow through the pump passages. The pump internal geometry is shown in figure 11. At very low frequencies, the division of flow among the impeller passages is nearly the same as the steady-state flow division. This division tends to minimize the overall resistance. At high frequencies, inertance becomes important. The flow from the passages in front of the diffuser tongue takes a short, low-inertance path through the volute, as shown by the streamline labeled A in figure 11. The flow from passages behind the tongue take long, high-inertance paths, as shown by streamline B. The high-frequency, perturbed flow travels more easily along the short, low-inertance paths. Thus, most of the flow will choose these paths, resulting in a flow distribution which tends to minimize the overall inertance, but which increases the overall resistance. This reasoning indicates that the resistance would tend to increase and the inertance to decrease with increasing frequency.

At a high enough frequency, the flow distribution is determined mainly by inertance, with resistance having a relatively small effect. In such a case, a further increase in frequency will not change the flow distribution very much. This would explain why the changes in the data are small above 20 hertz. This high-frequency regime might be called inertance controlled.

A change in the steady-state flow rate appears to affect the inertance values L_{6-8}, L_{6-9}, and L_{8-9} more at low frequencies than at high frequencies. This also can be explained as a result of the flow distribution inside the pump. Changing the steady-state flow rate changes the resistances of the impeller passages. Whereas a change in frequency affects the perturbed flow distribution through changes in the inertive reactances, a change in flow rate affects the flow distribution through changes in resistance. It is the relative sizes of the various resistances and reactances in the impeller and volute which determine the flow distribution. As mentioned before, the effects of inertance overshadow the effects of resistance at high frequencies. Consequently, the changes in the impeller resistances affect the flow distribution more at low frequencies than at high frequencies. One result is that the overall inertance values, which are affected by the flow distribution, would tend to show greater differences at low frequencies than at high frequencies.

At high frequencies, the differences become less than the data scatter, and the inertances approach common values which are unaffected by flow rate. In evaluating the inertance data at the flow coefficient of 0.497, it is useful to compare the high-frequency inertances to these common inertance values. At this flow coefficient, a systematic difference between the open-orifice and blocked-orifice inertances was noted in the section Data consistency. The present comparison shows that this difference is probably due to errors in the blocked-orifice data, since the open-orifice data agree better with the common inertance values.

At a flow coefficient of 0.442, the diffuser inertance L_{8-9} is constant within the accuracy of the data (fig. 10(b)). This shows that the diffuser is acting as a simple inertance element. The inertance can theoretically be calculated from the passage geometry by using the formula

$$L_{B-C} = \rho \int_{B}^{C} \frac{d\ell}{A} \tag{9}$$

where $d\ell$ denotes an increment of passage length, A the cross-sectional area at position ℓ, and B and C the beginning and end of the passage. The inertance computed by using this formula is shown as a solid line in figure 10(b). The agreement with the data at a flow coefficient of 0.442 is very good.

At the other flow coefficients, L_{8-9} deviates from the simple inertance model at low frequencies. It does not seem possible for the inertance to actually decrease below the theoretical value, as indicated. The average inertance would increase for any change in the flow distribution from the uniform flow assumed in deriving equation (9). Therefore, it is suspected that the pressure measured at the diffuser inlet is not repre-

sentative of the average pressure at that location. At high flow coefficients, the flow entering the diffuser has high velocities near the tongue and low velocities near the outer casing. The static-pressure tap at measuring station 8 is located near the outer radius; so for nonuniform flow distributions, the measured pressure might differ significantly from the average pressure. At measuring station 9 (the diffuser outlet), the velocity head is much smaller than at measuring station 8; furthermore, a nonuniform flow distribution would probably smooth out by the time it passed through the diffuser. Consequently, the measurements at station 9 are regarded as more reliable than those at station 8, and the R_{6-9} and L_{6-9} values are considered to be more accurate than R_{6-8}, R_{8-9}, L_{6-8}, and L_{8-9}.

At low frequencies, R_{8-9} is nearly constant for the flow coefficient of 0.442, but decreases with increasing frequency for the other flow coefficients. The diffuser resistance is basically caused by losses. One possible loss mechanism which would explain the observed trends is separated flow past the volute tongue. (Resistance is not proportional to loss, but to the derivative of loss with flow rate. But the resistance tends to be high when losses are high). At high flows, the radial velocities near the tongue become much higher than their design values, so that the tongue operates far from its design incidence angle. This would cause the losses to increase with flow rate at low frequencies. Studies of airfoils in unsteady flow have shown that the tendency to stall decreases with frequency, so the losses would decrease with frequency. At high frequencies, the trends are different. R_{8-9} tends to increase with frequency at all three flow coefficients, and does not appear to be affected by flow rate. Since the perturbed flow distribution is determined mainly by inertance at high frequencies, the overall flow rate has only a minor effect on the data.

To summarize, at the flow coefficient of 0.442, which is the one closest to the design flow coefficient, the dynamic behavior of the diffuser is simple and straightforward. The inertance is constant and can be computed from the diffuser geometry, while the resistance is constant (below 30 Hz) and equal to the steady-state value R_{SS}. However, at the two higher flow coefficients, the low-frequency trends are not so predictable. The reason for this may be the effects of the nonuniform flow distribution entering the diffuser.

Pump Dynamic Performance Model

A dynamic flow model can be developed for the pump by representing its component parts in terms of resistance and inertance. It has already been shown that the conical diffuser follows the simple, constant-resistance, constant-inertance model near design flow. The pump impeller and volute are a much more complicated case than the conical diffuser was, as there are 28 separate impeller passages, each emptying into the volute

at a different place. Each passage can be represented by an appropriate resistance and inertance in an electric circuit model of the pump. The impeller passages are treated as if they were not moving. It is shown in appendix B that for a radial-vaned impeller the inertance equation is the same whether the blades are moving or stationary. This is not true for a mixed-flow impeller.

Electric circuit model of pump. - The pump passages are shown schematically in figure 11, and the electrical circuit model of the pump is shown in figure 12. Each of the 28 impeller passages is represented by an inertance L_1 and a resistance R_1. The volute is represented by the circuit elements R_{Ai} and L_{Ai}, with i ranging from 1 to 27. The elements R_{Ai} and L_{Ai} represent the resistance and inertance experienced by the volute flow in going from the outlet of one impeller passage to the outlet of the next passage. The elements R_{A28} and L_{A28} represent the conical diffuser. Measurement station 9, located at the outlet of the diffuser, corresponds to the point having voltage E_{A29} in the circuit. Measurement station 8 is just before the diffuser inlet, the point having voltage E_{A28} in the circuit.

The representation of the flow passages by resistances and inertances is based on the assumption of a one-dimensional flow. The model requires that the flow conditions at any θ-coordinate of the volute be described by a single value of pressure and a single value of flow rate. Because of this requirement, the effects of radial pressure and flow variations can not be accounted for. The flow leaving each impeller passage is assumed to mix immediately with the flow already in the volute, whereas the actual case is more complicated. The model is intended to be only a relatively simple, approximate predictor of the pump dynamic response.

The network of figure 12 was solved proceeding from left to right. Starting with a unit voltage for E_{A1}, the current through R_1 and L_1 (representing the first impeller passage) is computed. This current passes through R_{A1} and L_{A1} (representing the volute impedance), allowing the voltage difference between E_{A2} and E_{A1} to be determined. From E_{A2}, the current in the second branch of the circuit is determined. Continuing this calculation through all 28 branches of the circuit would be tedious, so the solution was programmed on a digital computer. The important results in this calculation are the overall impedances. The impedance Z_{6-8}, representing the response of the impeller and the volute, is equal to the voltage E_{A28} divided by the total current (the current through R_{A28} and L_{A28}). The impedance Z_{6-9}, representing the response of the entire pump, is equal to E_{A29} divided by the total current.

One effect of a change in frequency is to change the distribution of current in the network. The current distributions are compared in figure 13, which shows the magnitudes of the currents in the branches of the circuit which represent the impeller passages. The results are normalized by dividing the currents by the total current which flows through R_{A28} and L_{A28}. The total current decreases with increasing frequency for a constant overall voltage, because of the increase in the inertive reactances. At higher

frequencies, most of the current flows through the higher numbered branches of the network. In hydraulic terms, this means that the perturbed flow is concentrated in the passages just before the tongue, as was mentioned previously. It is these changes in the perturbed flow distribution which are responsible for the changes in the overall resistance and inertance with frequency.

The current distributions of figure 13 are for a case where the resistances from R_{A1} to R_{A27} were zero (the same case as was used to compute the zero-R_{Ai} curve of fig. 14). The zero-R_{Ai} case was chosen for this example since it best illustrates what actually happens in the pump as frequency changes. This case had equal flow in all passages at zero frequency, which approximates the actual steady-state flow distribution close to design flow. Using nonzero R_{Ai} values resulted in unrealistic flow distributions at zero frequency.

Selection of resistance and inertance values. - To use the model requires a knowledge of what the values of R_1, L_1, R_{Ai}, and L_{Ai} should be. While the inertance values can be computed from the pump geometry, there was some question as to the best choice for the resistance values. Several choices of resistance values were tried, and the results were compared to the measured impedance data. What was desired was a relatively simple method of choosing the resistance values which would give a reasonably good data fit. How the inertance and resistance values were actually determined is discussed in detail in the following paragraphs. Once a method is developed for determining all the parameters in the model, it can hopefully be applied to other pumps for which dynamic data are not available.

The inertance values were calculated from flow passage geometry by using equation (9). The diffuser inertance L_{A28} was 152 900 newton-second^2 per meter^5 (90.4 lbf-sec^2/ft^5); this is the theoretical inertance value shown in figure 10(b). The impeller passage inertance L_1 was 720 000 newton-second^2 per meter^5 (426 lbf-sec^2/ft^5), while the volute inertances ranged from an L_{A1} value of 222 000 (131) to the L_{27} value of 17 500 (10.36). Even though the impeller passages were of different lengths due to the use of splitter blades, a single inertance value, based on the length of the main blade, was used for all. The inertance L_1 also includes the inertance of a vaneless diffuser section, a narrow (0.635 cm by 2.54 cm, or 1/4 in. by 1 in.) passage above which the passage widens out to form the volute. The model requires that the flow be regarded as independent of the volute flow to a certain point, and completely mixed with the volute flow beyond that point. The flow out of a pump passage will actually take a little time to conform to the volute flow; so the dividing point was chosen to be somewhat beyond the impeller outlet. The L_{Ai} values were calculated from the geometry of the volute (not including the vaneless diffuser section). The inertance values are inversely proportional to cross-sectional area, and are consequently high in the narrow part of the volute just behind the tongue, and low just in front of the tongue.

The values of R_1 and R_{Ai} can be chosen to match a given overall resistance value at a specified frequency. However, there are always many combinations of R_1 and R_{Ai} values which will do that. The effects of changing the relative sizes of the R_{Ai} values compared to R_1 are shown in figure 14. An estimate was made of the resistances occurring in the impeller and the volute, with the narrowest part of the volute assumed to have the highest R_{Ai} values. This case is identified in figure 14 as the "first estimate of R_{Ai} values." For the second case (reduced R_{Ai} values) the ratios R_{Ai}/R_1 were one-half those of the first case. For the third case (zero R_{Ai} values), all R_{Ai} values except R_{A28} (the diffuser resistance) are zero. The R_1 and R_{Ai} values were scaled to give the same overall resistance R_{6-8} of 6.26×10^6 N-sec/m^5 (3700 lbf-sec/ft^5) at 25 hertz. This resistance was chosen to match the data for the flow coefficient of 0.442.

The effects of changing the ratios R_{Ai}/R_1 were important only at low frequencies. The zero-R_{Ai} case had the greatest changes in both R_{6-8} and L_{6-8} between low frequencies and high frequencies. This case also fit the experimental data best at the flow coefficient (0.442) closest to the design flow, although it still underestimated the difference between the low-frequency and high-frequency R_{6-8} values. Because it is also the simplest case, the zero-R_{Ai} case was selected as the best choice to use with the model.

However, there is one point which should be considered since it casts a little doubt on the validity of the results shown in figure 14. The cases computed with nonzero R_{Ai} values had highly unlikely flow distributions. In one instance, the zero-frequency flow rate through passage 28 was over 100 times as great as the flow rate through passage 1. The question is whether these unrealistic flow splits jeopardize the results for the overall R and L values.

In order to see how a more reasonable flow distribution would affect the results, a second model was tried. The significant difference between the two models was that the one-dimensional-flow assumption of the first model, which made it impossible to consider the effects of radial pressure gradients in the volute, was discarded. In the second model, the flow from each impeller passage was represented by a separate streamline in the volute; this allowed the radial pressure variations to be considered. The flow rates in the second model were specified to be equal in all impeller passages at zero frequency. Although this is a much more realistic flow distribution than that of the first model, the overall R and L values computed from the two models were not very different. Because the items of interest are the overall R and L values and not the individual flow rates, the second model was discarded in favor of the simpler first model.

Comparison of model results to impedance data. - The results using the model are shown as solid lines in figures 8 and 9. The R_{Ai} values (except R_{A28}) were assumed to be zero, and R_1 was chosen to fit the R_{6-8} data. To test validity of the model, R_1 was chosen so that the overall resistance fit the data in the middle of the frequency

range, 25 hertz. The diffuser resistance R_{A28} was chosen to fit the R_{8-9} data. Different values of R_1 and R_{A28} were required at each different flow coefficient. The model gave reasonably good curve fits for the R_{6-8} and L_{6-8} data of figure 9. It also agreed with the data for the entire pump (fig. 8) at the flow coefficient of 0.442. However, it did not agree with the low-frequency results at the other two flows. The lack of agreement is due to the deviation of the diffuser parameters R_{8-9} and L_{8-9} from the values assumed in the model. In general, the low-frequency results for these parameters are hard to explain and may be in error, as previously discussed. More study is needed on how L_{8-9} and R_{8-9} vary with frequency.

Application of model using steady-state data. - The model would not be very useful unless it could be used when dynamic data are not available. In this case, a different method of determining R_1 and R_{A28} is necessary. The resistance R_1 can be obtained from R_{SS}, which is proportional to the slope of the steady-state head-flow curve. For the zero-R_{Ai} case, R_1 is equal to R_{SS} times the number of impeller passages, since for this case the circuit of figure 12 becomes a simple parallel circuit at zero frequency. The resistance R_{A28} is simply set equal to its steady-state value. Since the inertance values are computed from pump geometry, this means that the dynamic performance of a pump can be computed when only steady-state data are available.

The results based on the steady-state resistance values are shown as dashed lines in figures 8 and 9. The agreement with the R_{6-8} and R_{6-9} data is best at the flow coefficient (0.442) nearest the design flow. An inaccuracy in the steady-state R_{6-8} value might account for most of the differences between the model results and the data. At the higher flow coefficients, the model overestimates the resistance values. In figure 9(a); an inaccuracy either in the steady-state R_{6-8} value or in the model at zero frequency would throw the results off at all frequencies. At the two higher flow coefficients, the inaccuracies in the model (as judged from the solid lines) are at least as important as the inaccuracies in R_{SS}. The inaccuracies in the R_{8-9} values used in the model are just as great as the inaccuracies in R_{6-8} at the higher flow coefficients; both affect the R_{6-9} comparison of figure 9(a). The assumption that R_{8-9} is constant is a poor one at the higher flows.

The agreement with the inertance data is better than with the resistance data, although the low-frequency L_{6-9} agreement is affected by the discrepancies in L_{8-9}. The agreement of the model results with both the L_{6-8} and the L_{6-9} data is best at high frequencies. Furthermore, the inertive component of impedance becomes large compared to the resistance at high frequencies. This means that the model predicts the magnitude and phase of Z_{6-8} and Z_{6-9} more accurately at high frequencies.

In summary, the flow model developed herein gave a reasonable prediction of the trends of pump impedance with frequency. It gave the best results at high frequencies and at the flow coefficient of 0.442. The results are the most predictable at this flow

coefficient presumably because it is the closest to design flow, and consequently comes closest to having a uniform flow distribution in the impeller and volute. Obviously, before the general usefulness of the model can be assessed, it must be applied to other pump configurations. However, the results for this one set of pump data have been encouraging, particularly since the model provided reasonable estimates of pump impedance over a wide range of frequencies based only on pump geometry and steady-state flow measurements.

Pump Gain

Gain is generally assumed to be zero under noncavitating conditions. Since only a minute amount of tip vortex cavitation was present in the tests, the gain is expected to be very small. On the other hand, the method developed in reference 4 to determine gain (eq. (8)) is very sensitive to measurement errors. Thus the calculation of gain can be regarded as a check of the accuracy of the method of reference 4 as well as a check of the zero-gain assumption. The significance of the results can be judged with the help of an error analysis. The error analysis shows how much inaccuracy to expect in the computed gain values as a consequence of normal measurement errors.

The values of gain computed for the entire pump are shown in figure 15 for all three flow coefficients. The discharge pressure P_D corresponds to P_9, the suction pressure P_S to P_6. (Gain can also be computed for the impeller-volute combination, using P_8 for P_D. The P_9 results are shown here because the measurement of P_9 is considered more reliable than the measurement of P_8.) The gain values are seen to be

TABLE I. - PROBABLE ERROR IN GAIN

Frequency, Hz	Root-mean-square error in gain for flow coefficient of -	
	0.442	0.536
2	0.13	0.41
8	.20	.19
14	.28	.26
20	.38	.40
30	.55	.39
36	1.33	1.35
40	1.29	1.44
45	2.20	1.66

close to zero at low frequencies, but to diverge at high frequencies.

In order to see whether the results are consistent with the assumption that gain is zero, an error analysis was done. The details of the error analysis are given in appendix C. The results are shown in table I.

In general, the data points in figure 15 differ from zero by roughly the estimated error. The gain gets large just where the error analysis says it should, above 30 hertz. These results provide evidence that the observed trends in gain are due primarily to measurement errors, and that the error analysis provides an indication of the accuracy of the gain calculation method of reference 4.

Gain can be checked in another way. The impedances calculated from the blocked-orifice and open-orifice data would not be expected to show close agreement if gain were significantly different from zero. Therefore, the effect gain would have on the value of Z_{nc} will be examined. Equation (2) defines Z_{nc}, the impedance computed assuming zero gain, as

$$Z_{nc} = \frac{P_S - P_D}{Q_{out}} \tag{2}$$

The suction pressure is given by

$$P_S = \frac{1}{m + 1}(P_D + ZQ_{out}) \tag{10}$$

This is simply a rearranged form of equation (1). The ratio of P_D to Q_{out} is set by the exit impedance Z_e,

$$P_D = Z_e Q_{out} \tag{11}$$

Substituting equations (10) and (11) into equation (2),

$$Z_{nc} = \frac{1}{m + 1}(Z - mZ_e) \tag{12}$$

The difference between Z_{nc} for the open orifice and the blocked orifice is given by

$$Z_{nc,O} - Z_{nc,B} = \frac{m}{m + 1}(Z_{e,B} - Z_{e,O}) \tag{13}$$

Of course, measurement errors also produce differences between $Z_{nc,O}$ and $Z_{nc,B}$. But if it is assumed that the data scatter is caused entirely by nonzero gain values, an upper limit to the magnitude of the gain can be computed. This was done for the flow coefficient of 0.442 assuming a 5-percent difference, about the average data scatter, between $Z_{nc,O}$ and $Z_{nc,B}$. (The real part of Z_{nc} is R_{6-9}, the imaginary part is $2\pi fL_{6-9}$; the data scatter can be judged from fig. 8.) The exit impedance had a real part of about 6.59×10^6 N-sec/m^5 (3900 lbf-sec/ft^5) for the open-orifice case and about 10.65×10^6 (6300) for the blocked-orifice case. The imaginary part was the same for both cases.

The magnitude of the gain which would explain the data scatter is shown in table II.

TABLE II. - MAXIMUM GAIN CONSISTENT WITH THE AGREEMENT OF BLOCKED-ORIFICE AND OPEN-ORIFICE DATA

Frequency, Hz	Magnitude of maximum probable gain
2	0.09
8	.20
20	.42
32	.66
45	.92

It can be said that, based on the data alone, the gain is not greater than these values. Furthermore, there is nothing in the data to suggest that the gain is other than the theoretically assumed value of zero.

SUMMARY OF RESULTS

The dynamic performance of a radial-bladed centrifugal pump was measured using noncavitating inlet pressures. The results were analyzed in terms of resistance and inertance; this is normal procedure for a hydraulic system. Some of the results were

1. The reactance is important at all frequencies and is greater than the resistance except at relatively low frequencies (below 3 to 9 Hz, depending on the flow rate).

2. The resistance values calculated from the steady-state performance curves agreed reasonably well with the dynamic resistance data extrapolated to zero frequency.

3. Both resistance and inertance are frequency dependent. They change most rapidly at low frequencies; above 20 hertz, the changes are small. For the impeller-volute combination, the resistance increases with frequency, while the inertance decreases.

4. At the flow rate nearest the design flow, the inertance data for the outlet diffuser agreed very well with the inertance computed from the diffuser geometry. The diffuser resistance was constant (below 30 Hz) and equal to the steady-state value. At higher flows, some unexpected trends occurred at low frequencies, possibly caused by the non-uniform flow distribution at the diffuser inlet.

A model was developed in order to explain the trends of resistance and inertance with frequency. In this model, the pump is represented by an electric circuit. The model does not require any dynamic data; inertances are computed from pump passage geometry, resistances from the steady-state performance curves. The results using the model showed good agreement with the data at the flow closest to the design flow.

The agreement is not as good at the higher flows, presumably because the performance is affected by the uneven flow distribution in the impeller and the volute. At these higher flows, the model gave reasonably accurate predictions of overall pump impedance at high frequencies, but not at low frequencies. The model overestimated the overall resistance values at almost all frequencies. This happened because the model assumed the individual passage resistances are constant, whereas they are actually frequency dependent. To improve the model results would require a better understanding of the losses due to off-design flow patterns. The inaccuracies in resistance are not critical at high frequencies, where the inertive reactance is the main component of pump impedance. The model results agreed with the inertance data better at high frequencies than at low frequencies. The discrepancies in the diffuser inertance at low frequencies and high flows also merit further investigation.

The data were also used to calculate gain. This was done both as a check on the method developed for determining gain and as a check on the assumption of zero gain. The gain was found to be zero within the accuracy of the measurements as shown by an error analysis. The error analysis also showed that the gain calculation is very sensitive to measurement errors.

Lewis Research Center,
National Aeronautics and Space Administration,
Cleveland, Ohio, August 23, 1971,
128-31.

APPENDIX A

SYMBOLS

A	cross-sectional area, m^2 (ft^2)
E	voltage
$\overline{F}$	blade force vector
f	perturbation frequency, Hz
j	imaginary unit, $\sqrt{-1}$
L	inertance, N-sec^2/m^5 (lbf-sec^2/ft^5)
l	length coordinate
$\overline{l}$	direction of blade passage
m	gain (see eq. (1))
P	perturbed total pressure, N/m^2 (lbf/ft^2)
p	perturbed static pressure, N/m^2 (lbf/ft^2)
Q	perturbed flow rate, m^3/sec (ft^3/sec)
Q_{av}	steady-state flow rate, m^3/sec (ft^3/sec)
R	resistance, N-sec/m^5 (lbf-sec/ft^5)
$\overline{r}$	radius vector
t	time, sec
U	wheel speed, m/sec (ft/sec)
V	velocity, m/sec (ft/sec)
W	relative velocity, m/sec (ft/sec)
X	reactance, N-sec/m^5 (lbf-sec/ft^5)
x	length coordinate, m (ft)
Z	impedance, N-sec/m^5 (lbf-sec/ft^5)
Δ	finite difference or, in appendix C, magnitude of a random error
ρ	density, kg/m^3 ($slug/ft^3$)
$\overline{\varphi}$	flow coefficient (ratio of average inlet flow velocity to blade tip speed)
ψ	head-rise coefficient
ω	rotor rotational speed, rad/sec

ω'	2π times perturbation frequency

Subscripts:

A	volute circuit component in fig. 12
av	average
B	blocked orifice
D	discharge (either measurement station 8 or station 9)
e	exit
i	branch of network, ranges from 1 to 28
in	inlet
nc	noncavitating
O	open orifice
or	orifice
out	outlet (measurement station 9)
R	relative to moving coordinate system
S	suction
SS	computed from steady-state data
θ	peripheral coordinate
1	impeller passage circuit component in fig. 12
1,2	beginning and end of flow passage, appendix B
5,6,8, 9,10	measurement station locations, fig. 1 (A double subscript separated by a hyphen (as in Z_{6-9}) refers to the flow passage between the respective measurement stations.)

Superscript:

	perturbation quantity

APPENDIX B

DERIVATION OF INERTANCE EQUATION

The inertance equation is usually derived for a quiescent fluid with stationary boundaries. The first part of this appendix derives the inertance equation for the case of a flowing fluid. The second part considers the case where both the fluid and the boundaries are moving.

Derivation of Inertance Equation for Stationary Boundaries

The analogy between fluid inertance and electrical inductance is commonly used in the field of acoustics. The inertance equation, on which this analogy is based, is usually derived for the case of a disturbance acting on a fluid at rest. The following derivation considers the case of a disturbance superimposed on a fluid in motion. The result is an equation having the same form as the usual inertance equation, but using total pressure instead of static pressure.

The equation of motion for a fluid, neglecting viscous terms, is (ref. 6, eq. 3(9), neglecting all forces except pressure)

$$\rho \frac{D\bar{V}}{Dt} = -\nabla p \tag{B1}$$

Applying this equation to a simple one-dimensional flow as shown in figure 16,

$$\rho\left(\frac{\partial V}{\partial t} + V\frac{\partial V}{\partial x}\right) = -\frac{\partial p}{\partial x} \tag{B2}$$

Making the following substitution

$$\frac{\partial P}{\partial x} = \frac{\partial}{\partial x}\left(p + \frac{1}{2}\rho V^2\right) = \frac{\partial p}{\partial x} + \rho V\frac{\partial V}{\partial x} \tag{B3}$$

gives the equation in terms of total pressure

$$\rho \frac{\partial V}{\partial t} = -\frac{\partial P}{\partial x} \tag{B4}$$

Now assume that V is composed of a steady-state component V_{av} and a perturbation component V', as given by the following equation:

$$V = V_{av} + V'e^{j\omega' t} \tag{B5}$$

In this equation, the phase differences in the perturbation term at different x-coordinates are neglected. This is a good approximation if the length of the passage is much shorter than one-quarter wavelength. A similar equation is assumed for P,

$$P = P_{av} + P'e^{j\omega' t} \tag{B6}$$

Substituting equations (B5) and (B6) into equation (B4) and separating out the time dependent terms yield

$$j\omega'\rho V' = -\frac{dP'}{dx} \tag{B7}$$

Integrating over the length of the passage (from x_1 to x_2),

$$-\int_{x_1}^{x_2} dP' = \int_{x_1}^{x_2} j\omega'\rho V'\, dx = j\omega' \int_{x_1}^{x_2} AV'\rho \frac{dx}{A} \tag{B8}$$

The mass flow $\rho AV'$ can be assumed to be constant if the passage is much shorter than one-quarter wavelength. Equation (B8) can then be written as

$$P'_1 - P'_2 = j\omega' AV'\rho \int_{x_1}^{x_2} \frac{dx}{A} \tag{B9}$$

This is the standard form of the inertance equation. The total pressure P' is analogous to voltage, the volumetric flow AV' to current, and the inertance $\rho \int dx/A$ to inductance.

Derivation of Inertance Equation for Rotor Passages

One form of the equation of motion for relative flow in a turbomachine is (ref. 6, eq. 7(39))

$$\frac{\partial_R \overline{W}}{\partial t} + \frac{1}{\rho} \nabla P_R = \overline{W} \times \left(\text{curl } \overline{W} + 2\overline{\omega} \right) + \overline{F} \tag{B10}$$

where the relative total pressure P_R is given by (neglecting the gravitational force term)

$$P_R = p + \frac{1}{2} \rho \left[W^2 - \left(\overline{\omega} \times \overline{r} \right)^2 \right] \tag{B11}$$

Assume that there are a large number of blades and relatively narrow passages. The relative velocity $\overline{W}$ is constrained to flow in the direction of the blade passages. This direction is designated as $\overline{l}$ in figure 17. Since the vector $\overline{W} \times \left(\text{curl } \overline{W} + 2\overline{\omega} \right)$ is perpendicular to $\overline{W}$, it has no component in the $\overline{l}$ direction. Neglecting viscous forces, $\overline{F}$ represents the force exerted by the blades on the fluid. This force is normal to the blade surfaces, so it also has no component in the $\overline{l}$ direction. Consequently, the component of equation (B10) in the $\overline{l}$ direction is simply

$$\rho \frac{\partial_R W}{\partial t} = - \frac{\partial P_R}{\partial l} \tag{B12}$$

The quantities W and P_R can be assumed to be composed of a steady component and a perturbation component, as was done in the preceding section for V and P:

$$W = W_{av} + W' e^{j\omega' t} \tag{B13}$$

$$P_R = P_{R,av} + P'_R e^{j\omega' t} \tag{B14}$$

Note that ω and ω' are not the same; ω is the rate of rotation of the turbomachine in radians per second, while ω' is 2π times the perturbation frequency. Substituting equations (B13) and (B14) into equation (B12) and keeping only the time-dependent terms,

$$j\omega' \rho W' = -\frac{\partial P'_R}{\partial l} \tag{B15}$$

Integrating over the passage length yields

$$P'_{R,1} - P'_{R,2} = \int_{l_1}^{l_2} j\omega' A W' \rho \frac{dl}{A} = j\omega' A W' \rho \int_{l_1}^{l_2} \frac{dl}{A} \tag{B16}$$

However, to analyze a system containing both rotating and stationary flow passages would require that this equation be given in terms of absolute pressures and velocities. For velocities, the perturbed component is the same whether the flow is relative or absolute. Expanding the equation

$$\overline{V} = \overline{W} + \left(\overline{\omega} \times \overline{r}\right) \tag{B17}$$

in terms of steady and perturbed components (it is assumed that $\overline{\omega}$ is constant)

$$\overline{V}'_{av} + \overline{V}' e^{j\omega' t} = \overline{W}_{av} + \overline{W}' e^{j\omega' t} + \left(\overline{\omega} \times \overline{r}\right) \tag{B18}$$

Equating the two time-dependent terms,

$$\overline{V}' = \overline{W}' \tag{B19}$$

For pressures, start with the relation between total pressure and relative total pressure

$$P = p + \frac{1}{2}\rho\left[\overline{W} + \left(\overline{\omega} \times \overline{r}\right)\right]^2 = P_R - \frac{1}{2}\rho\left[W^2 - \left(\overline{\omega} \times \overline{r}\right)^2\right] + \frac{1}{2}\rho\left[\overline{W} + \left(\overline{\omega} \times \overline{r}\right)\right]^2$$

$$= P_R + \frac{1}{2}\rho\left[2\overline{W} \cdot \left(\overline{\omega} \times \overline{r}\right) + 2\left(\overline{\omega} \times \overline{r}\right)^2\right]$$

$$= P_R + \rho\left(UW_\theta + U^2\right) \tag{B20}$$

where U denotes the wheel speed which is the magnitude of $\overline{\omega} \times \overline{r}$ and W_θ is the component of $\overline{W}$ in the $\overline{\omega} \times \overline{r}$ direction.

In terms of steady-state and perturbed components,

$$P_{av} + P'e^{j\omega' t} = P_{R,av} + P'_R e^{j\omega' t} + \rho\left[U\left(W_{\theta,av} + W'_\theta e^{j\omega' t}\right) + U^2\right] \tag{B21}$$

Equating the perturbed components,

$$P' = P'_R + \rho U W'_\theta \tag{B22}$$

Substituting equations (B22) and (B19) into equation (B16),

$$P'_1 - \rho U_1 V'_{\theta,1} - P'_2 + \rho U_2 V'_{\theta,2} = j\omega' A V' \rho \int_{l_1}^{l_2} \frac{dl}{A} \tag{B23}$$

Unless there is turning upstream of the pump inlet, $V'_{\theta,1}$ will usually be zero. Furthermore, for a radial-vaned centrifugal pump, $V'_{\theta,2} = W'_{\theta,2} = 0$. Thus, for the test pump of this report, both V'_θ terms are zero, and equation (B23) becomes the same as the equation for stationary passages (eq. (B9)).

APPENDIX C

ERROR ANALYSIS OF GAIN CALCULATION

The effect of random measurement errors on the accuracy of the gain values can be determined by using the methods of reference 7. An equation can be derived giving the error in gain as a function of the errors in the individual measurements. Let f denote a function of the measured variables $x_1, x_2, \ldots, x_n$. If the errors are assumed to be random errors, the probable error in f is given by (ref. 7, eq. (3))

$$(\Delta f)^2 = \left(\frac{\partial f}{\partial x_1}\Delta x_1\right)^2 + \left(\frac{\partial f}{\partial x_2}\Delta x_2\right)^2 + \ldots + \left(\frac{\partial f}{\partial x_n}\Delta x_n\right)^2 \tag{C1}$$

where Δ denotes the magnitude of the respective error.

The function to be considered in this analysis is the gain m as given in equation (8)

$$m + 1 = \frac{P_{D,O}Q_B - P_{D,B}Q_O}{P_{S,O}Q_B - P_{S,B}Q_O} \tag{C2}$$

$$d(m+1) = \frac{1}{D^2}\Big[(DP_{D,O} - NP_{S,O})dQ_B - (DP_{D,B} - NP_{S,B})dQ_O$$

$$+ Q_B(D\,dP_{D,O} - N\,dP_{S,O}) - Q_O(D\,dP_{D,B} - N\,dP_{S,B})\Big] \tag{C3}$$

where N denotes the numerator of equation (C2), and D the denominator.

The perturbed flow rate Q is calculated from several measurements, one of which is P_D. So before equation (C1) can be applied, the errors in Q due to errors in P_D must be separated out and combined with the other terms containing dP_D. The two parts of dQ shall be written as

$$dQ = \frac{\partial Q}{\partial P_D}dP_D + dQ_{other} \tag{C4}$$

Applying equation (C1), the error equation for gain is

$$\Delta m^2 = \left[\frac{1}{|D|^4} |DP_{D,O} - NP_{S,O}|^2 \left(\Delta Q_{B,\text{other}}\right)^2 + |DP_{D,B} - NP_{S,B}|^2 \left(\Delta Q_{O,\text{other}}\right)^2 \right.$$

$$+ \left| DQ_B - (DP_{D,B} - NP_{S,B}) \frac{\partial Q_O}{\partial P_{D,O}} \right|^2 \left(\Delta P_{D,O}\right)^2 + |NQ_B|^2 \left(\Delta P_{S,O}\right)^2$$

$$\left. + \left| DQ_O - (DP_{D,O} - NP_{S,O}) \frac{\partial Q_B}{\partial P_{D,B}} \right|^2 \left(\Delta P_{D,B}\right)^2 + |NQ_O{}^2| \left(\Delta P_{S,B}\right)^2 \right] \qquad \text{(C5)}$$

Now consider the outlet flow rate Q more closely. It is calculated from

$$Q = \frac{\frac{1}{2}(p_9 - p_{10} + p_{9-10})}{\frac{2\,\Delta\overline{P}}{\overline{Q}} + j\omega' L_{9-10}} \qquad \text{(C6)}$$

where p_9 is the static perturbed pressure measured in front of the multihole orifice plate, p_{10} the pressure measured behind the orifice plate, and p_{9-10} a directly measured pressure difference across the orifice plate. Taking the derivative of this equation and dividing by Q gives

$$\frac{dQ}{Q} = \frac{dp_9 - dp_{10} + dp_{9-10}}{p_9 - p_{10} + p_{9-10}} - \frac{d\left(\frac{\Delta\overline{P}}{\overline{Q}}\right)}{\frac{\Delta\overline{P}}{\overline{Q}}} \qquad \text{(C7)}$$

The outlet line reactance $\omega' L_{9-10}$ is small compared to the multihole orifice resistance $2\,\Delta\overline{P}/\overline{Q}$, and has been neglected. Measuring station 9 is the discharge measuring station; so p_9 is the static-pressure component of the discharge total pressure P_D. The errors in the velocity head $P_D - p_9$ are small compared to the errors in p_9; so Δp_9 is approximately the same as ΔP_D. Consequently, the partial $\partial Q/\partial P_D$ is given by

$$\frac{\partial Q}{\partial P_D} = \frac{Q}{p_9 - p_{10} + p_{9-10}} = \frac{Q}{2p_{9-10}} \tag{C8}$$

(Since p_{9-10} is nearly equal to $p_9 - p_{10}$, the denominator equals $2p_{9-10}$ accurately enough for these calculations.) The other terms in equation (C7) combine to form ΔQ_{other}, which is given by

$$\frac{\left(\Delta Q_{other}\right)^2}{Q^2} = \frac{\left(\Delta p_{10}\right)^2 + \left(\Delta p_{9-10}\right)^2}{\left|2p_{9-10}\right|^2} + \frac{\left[\Delta\left(\frac{\Delta\overline{P}}{\overline{Q}}\right)\right]^2}{\left(\frac{\Delta\overline{P}}{\overline{Q}}\right)^2} \tag{C9}$$

Using equations (C5), (C8), and (C9), the error in gain can be calculated from estimates of the errors in the individual measurements. Two types of error were considered in estimating the amount of error in the perturbed pressures: (1) a 48-newton-per-square-meter (1-lbf/ft^2) error representing the background noise due to random pressure fluctuations, and so forth; and (2) an error of 2 percent of the measured value. These two errors were combined by using the sum-of-the-squares rule for random errors. The 48-newton-per-square-meter (1-lbf/ft^2) and 2-percent values are judgements based on experience with this type of measurement. The outlet orifice resistance $2\,\Delta\overline{P}/\overline{Q}$ was assumed to have a 2-percent error.

The results of the error analysis are shown in table I (RESULTS AND DISCUSSION section) of this report. A simplified form of equation (C5) was used in which it was assumed that N = D (i.e., that the gain is zero). The error in gain was found to be much greater at high frequencies than at low frequencies. The values in table I are highly approximate, and are intended to show mainly the order of magnitude of the errors. Because the two terms in the denominator of equation (C2) nearly cancel out, a relatively small change in any of the variables in the denominator could significantly affect the sensitivity of the gain to measurement errors. Also, the measurement error estimates are of a highly approximate nature.

REFERENCES

1. Rubin, S.: Instability Model of Missile Longitudinal Oscillation Due to Propulsion Feedback. Rep. TOR-269(4126)-28, Aerospace Corp., Sept. 21, 1964. (DDC No. AD-458211.)

2. Anon.: J-2 Vehicle Longitudinal Stability (POGO) Analysis Program. Rep. R-6283, Rocketdyne Div., North American Aviation (NASA CR-71905), Aug. 31, 1965.

3. Bikle, F. E.; Fidler, L. E.; and Rohrs, J. B.: A Study of System Coupled Instability Analysis Techniques. Pts. I and II. Rep. CR-66-36, Martin Co. (ARFPL-TR-66-143, AD-485312 and AD-485313), July 1966.

4. Stevans, William; and Blade, Robert J.: Experimental Evaluation of a Pump Test Facility with Controlled Perturbations of Inlet Flow. NASA TN D-6543, 1971.

5. Miller, Max J.; and Soltis, Richard F.: Detailed Performance of a Radial-Bladed Centrifugal Pump Impeller in Water. NASA TN D-4613, 1968.

6. Vavra, Michael H.: Aero-Thermodynamics and Flow in Turbomachines. John Wiley & Sons, Inc., 1960.

7. Anderson, Douglas A.: An Analysis of the Effect of Design and Measurement Errors on Pump Performance Parameters. NASA TN D-5919, 1970.

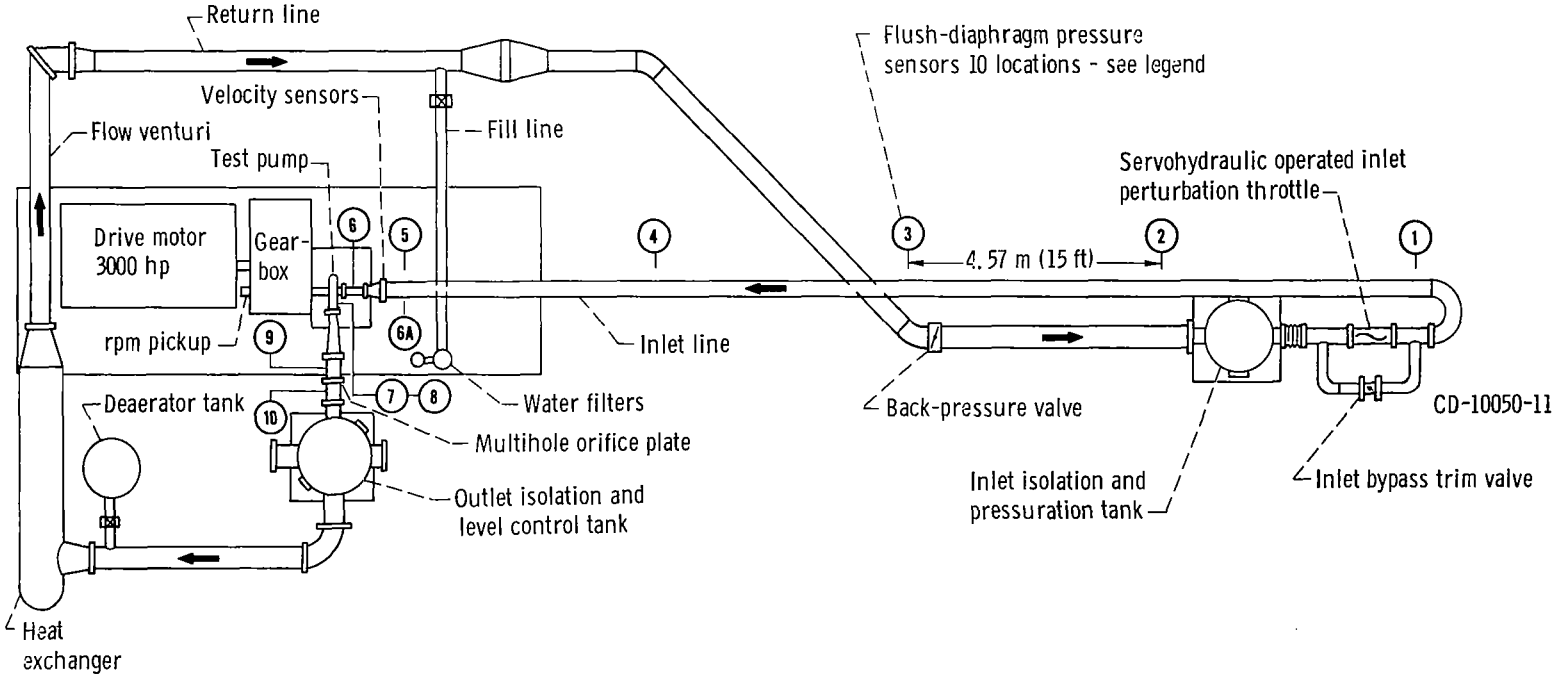

(a) General view of test facility.

Figure 1. - Pump Perturbations Test Facility, showing measuring stations. For analytical purposes, stations 1 to 5 and 6A are assumed to be attached to ground; stations 6 to 10 are assumed to be attached to the pump and pipe.

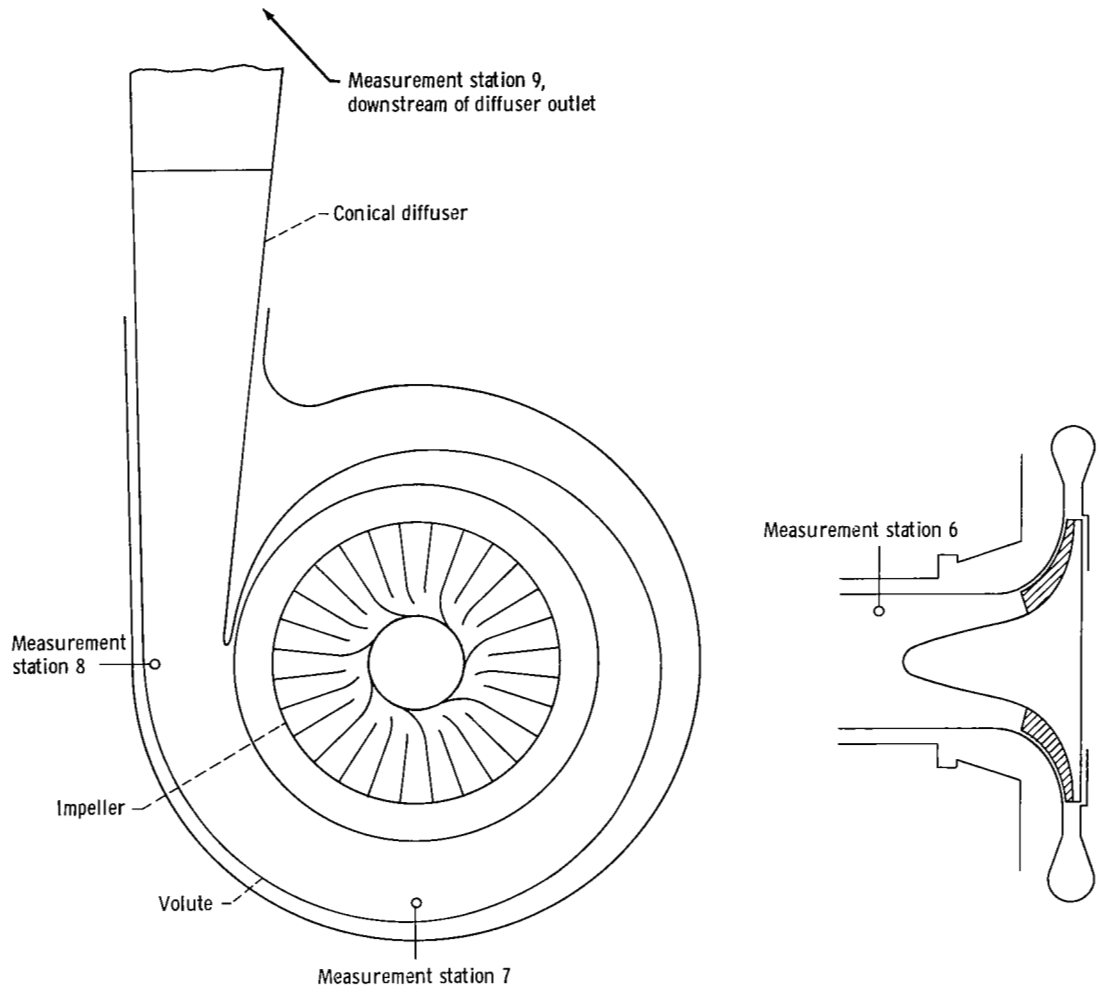

(b) Test pump, showing measurement stations.

Figure 1. - Concluded.

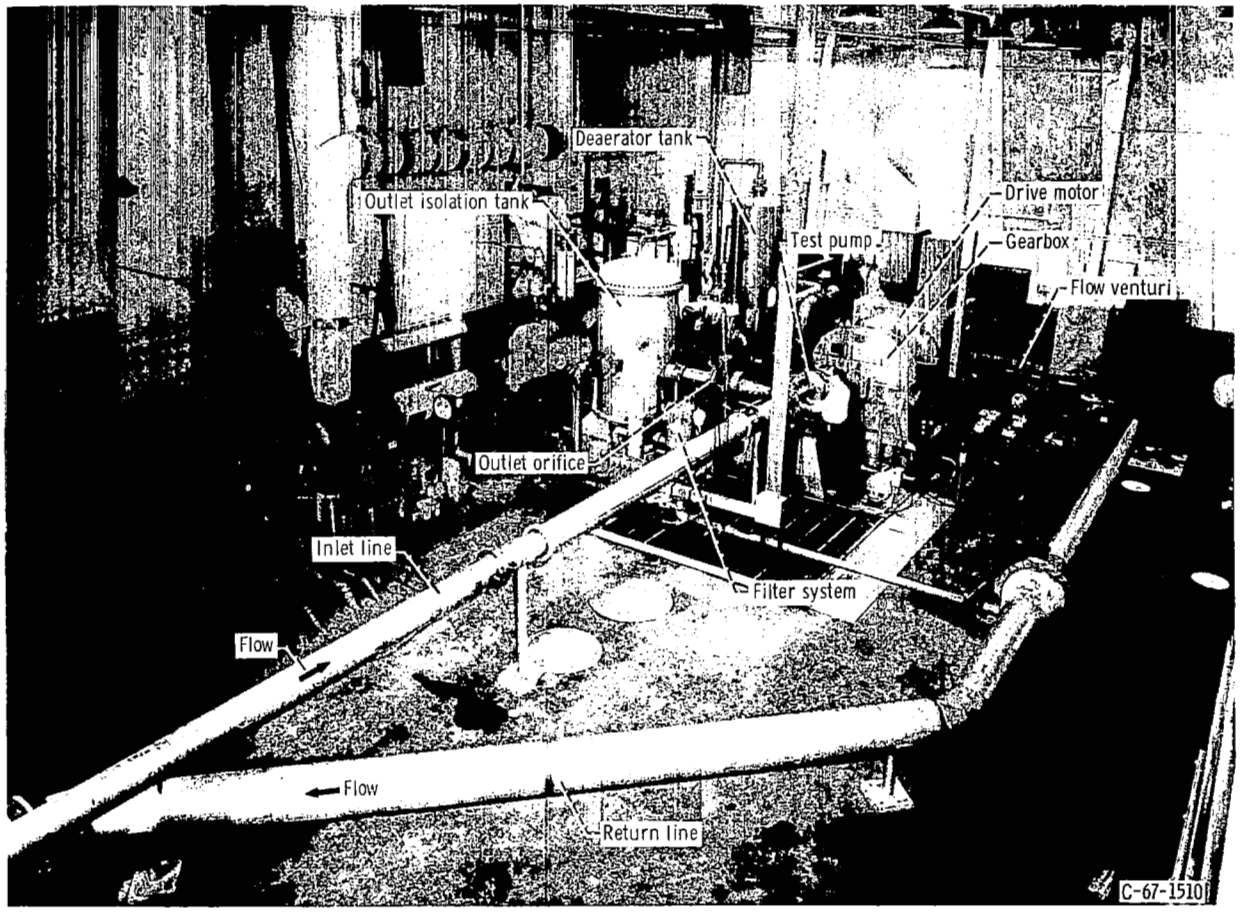

Figure 2. - Pump Perturbations Test Facility - interior of test cell.

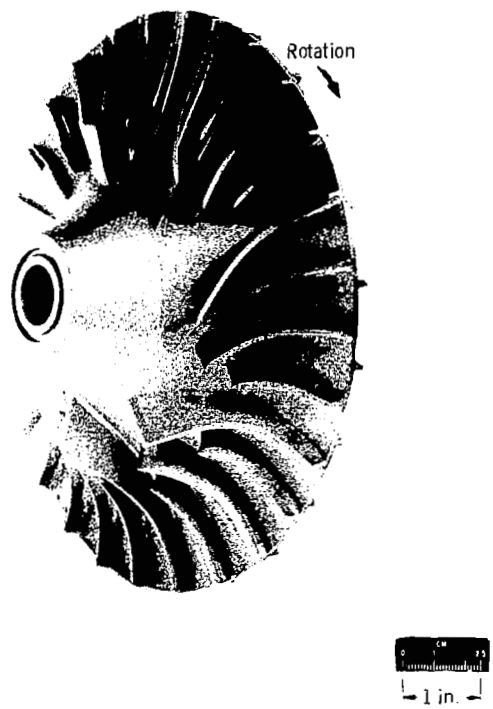

C-67-2902

Figure 3. - Radial-bladed centrifugal pump impeller.

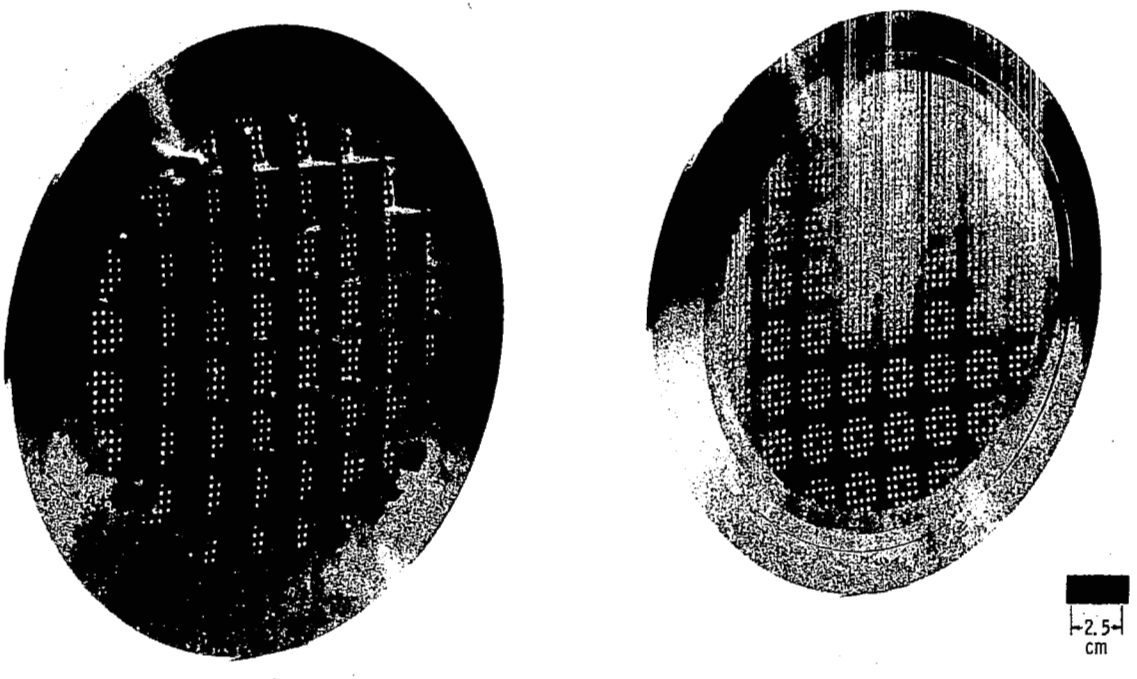

Back face

Front face

C-66-126

Figure 4. - Multihole orifice plate.

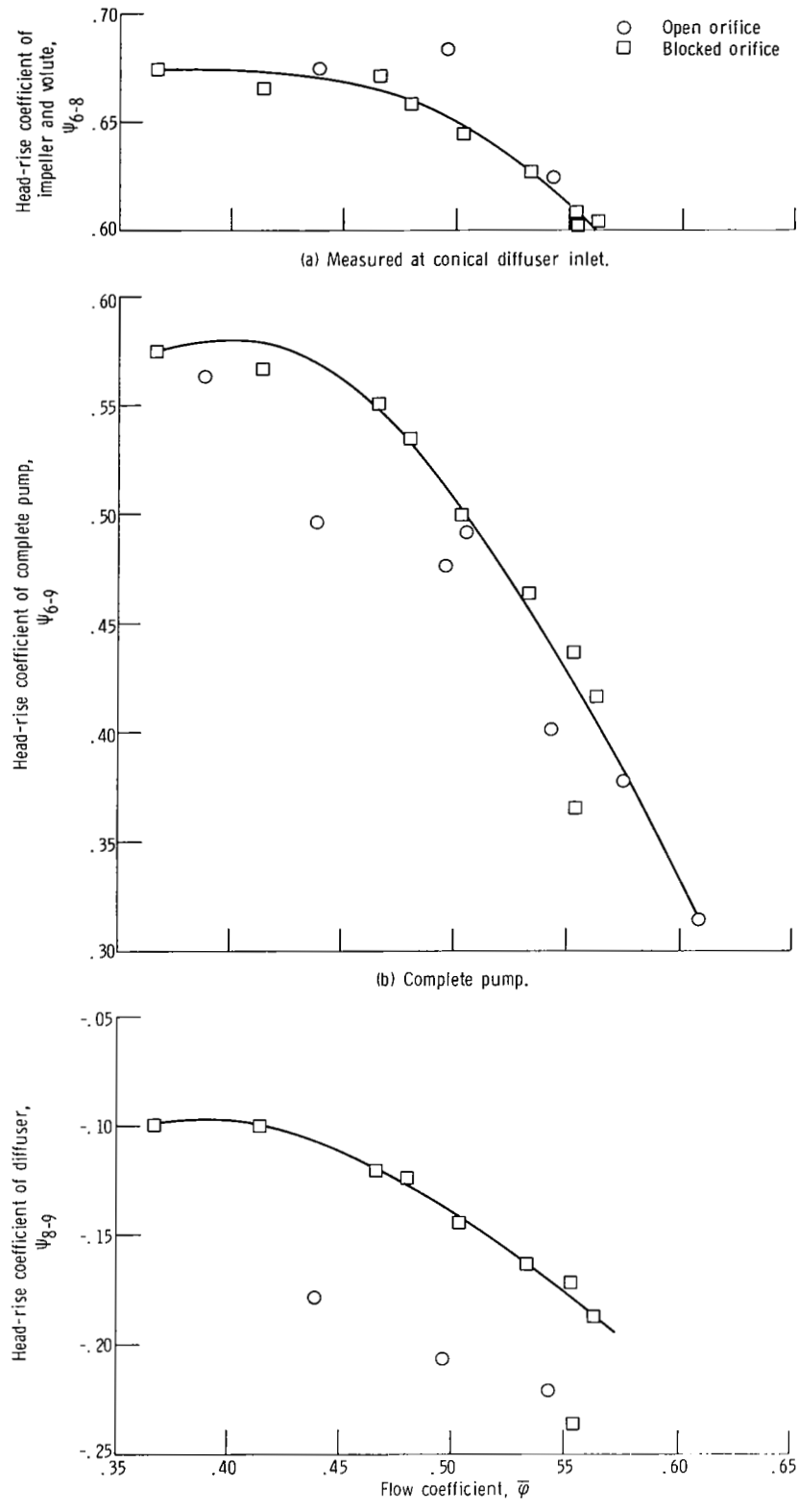

(a) Measured at conical diffuser inlet.

(b) Complete pump.

(c) Conical diffuser.

Figure 5. - Steady-state noncavitating performance of centrifugal pump.

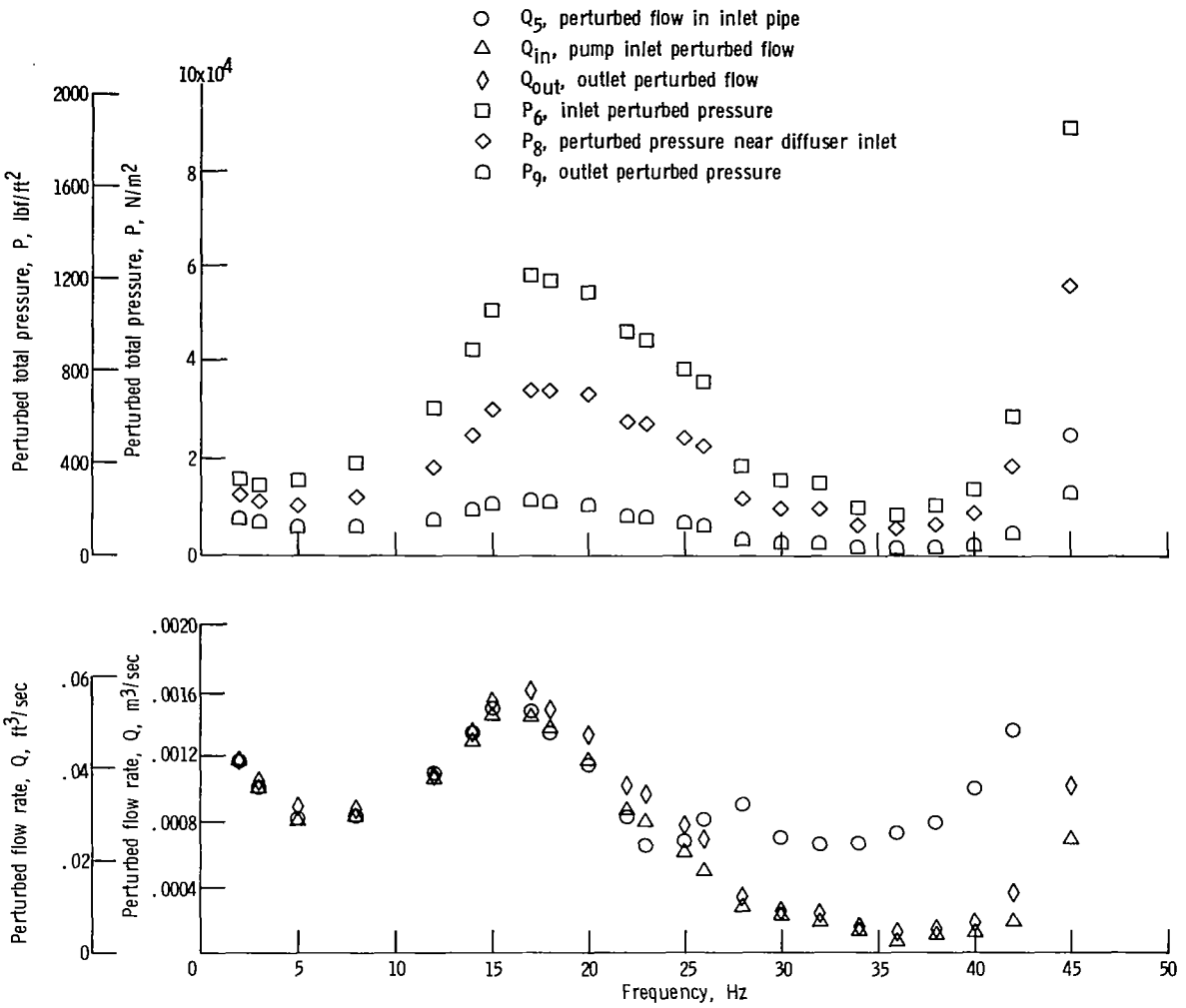

Figure 6. - Magnitude of perturbed pressures and flow rates. Flow coefficient, 0.442; open orifice.

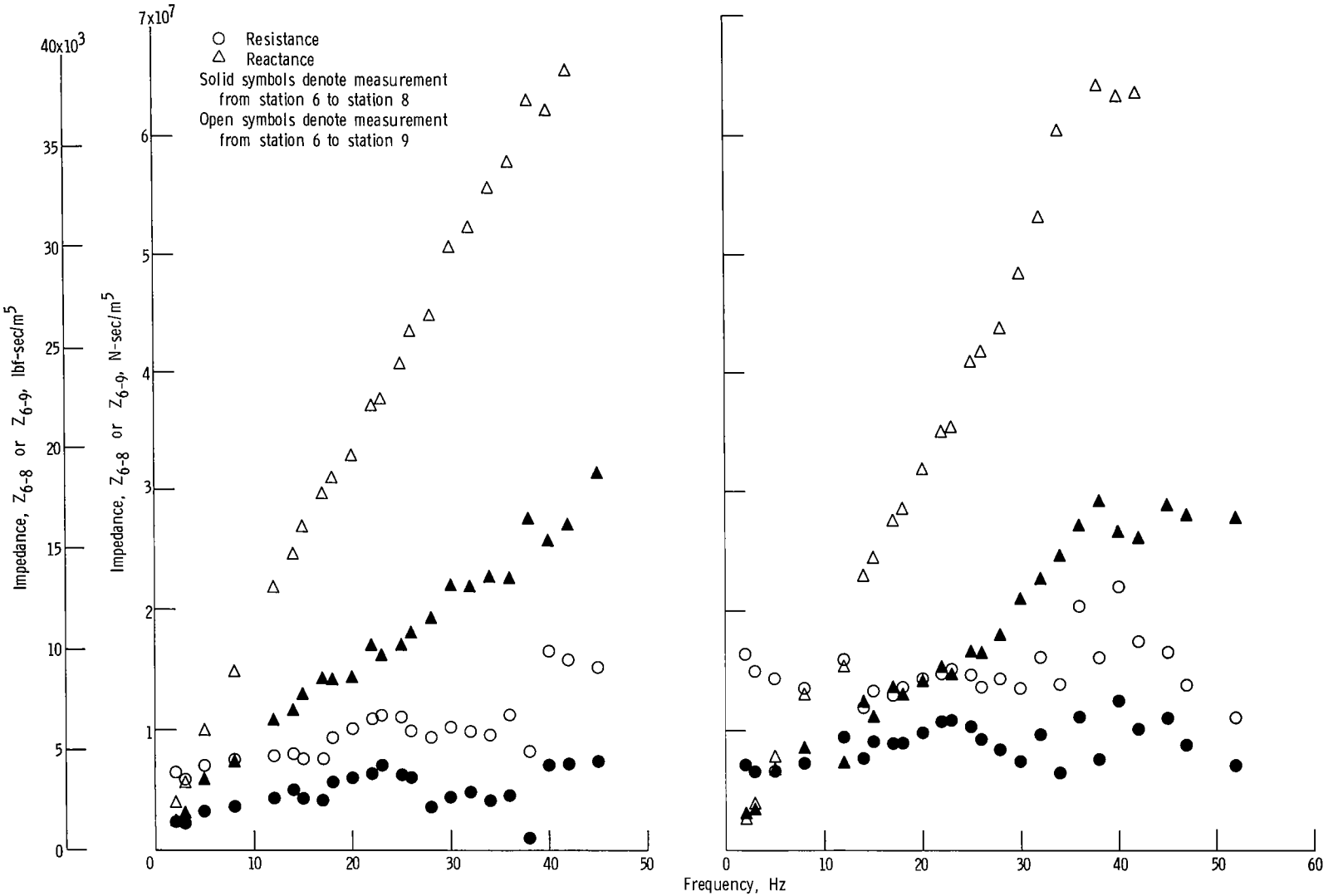

(a) Flow coefficient, 0.442.

(b) Flow coefficient, 0.536.

Figure 7. - Pump impedance - open-orifice data.

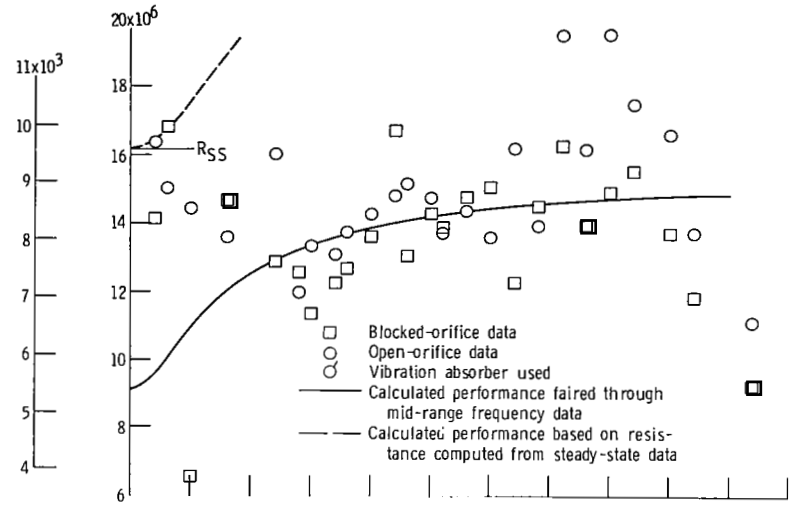

(a-1) Flow coefficient, 0.536.

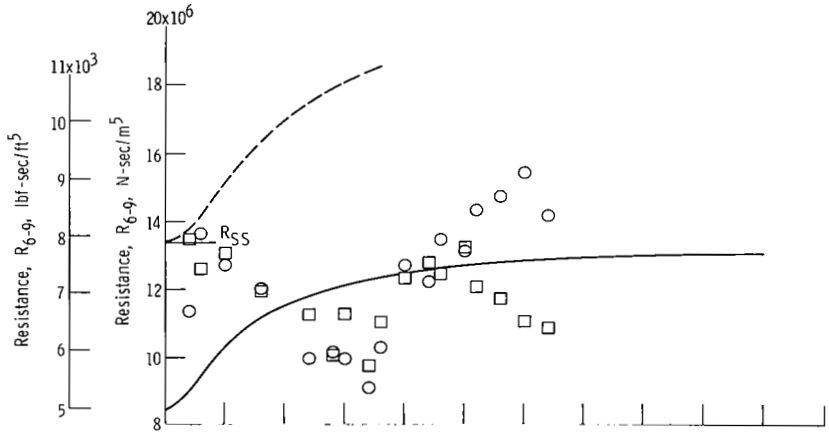

(a-2) Flow coefficient, 0.497.

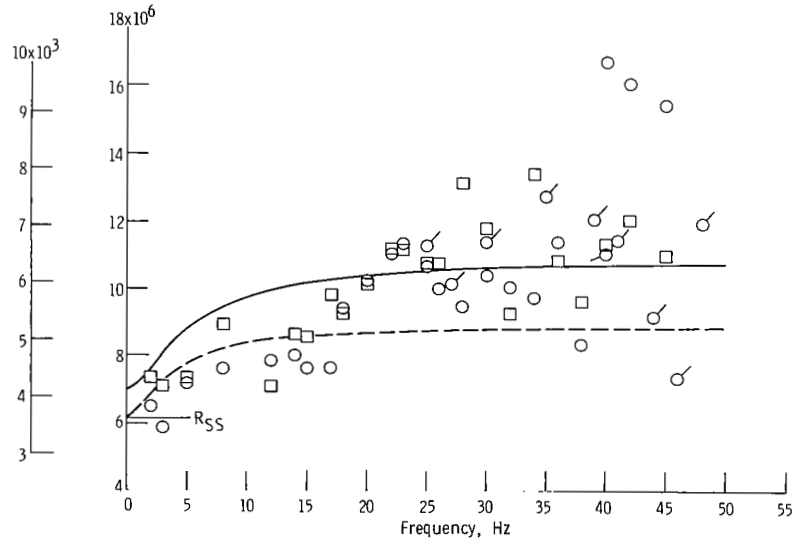

(a-3) Flow coefficient, 0.442.

(a) Resistance, R_{6-9}.

Figure 8. - Resistance and inertance across the complete pump.

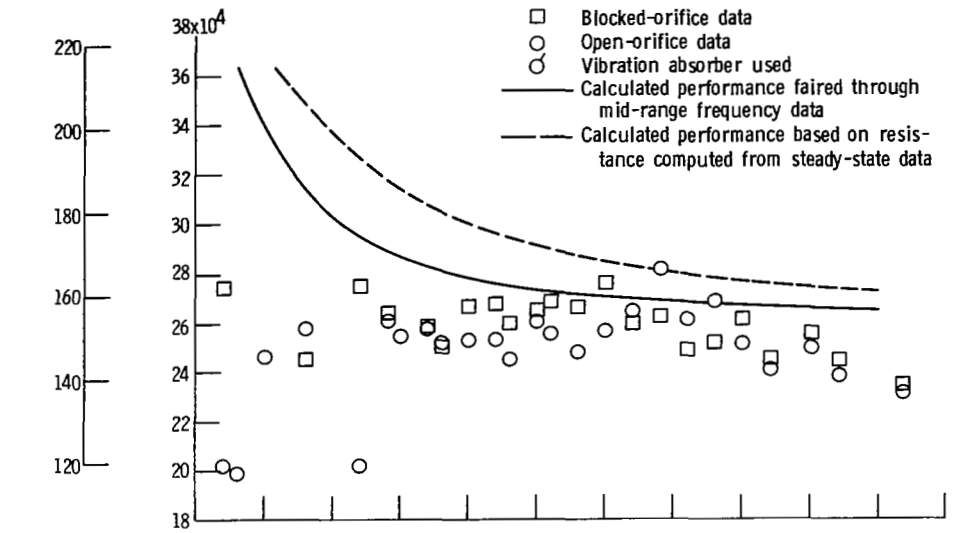

(b-1) Flow coefficient, 0.536.

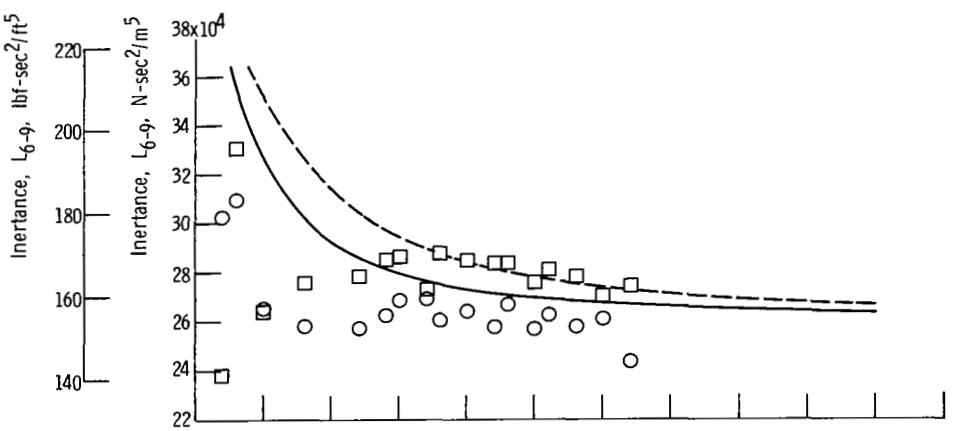

(b-2) Flow coefficient, 0.497.

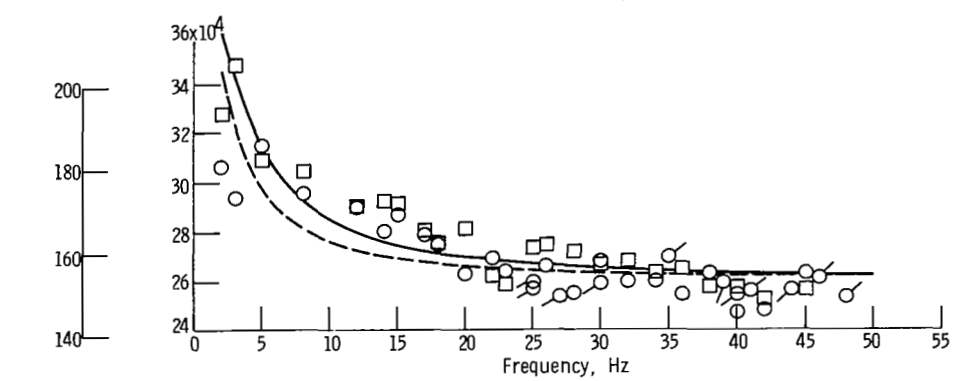

(b-3) Flow coefficient, 0.442.

(b) Inertance, L_{6-9}.

Figure 8. - Concluded.

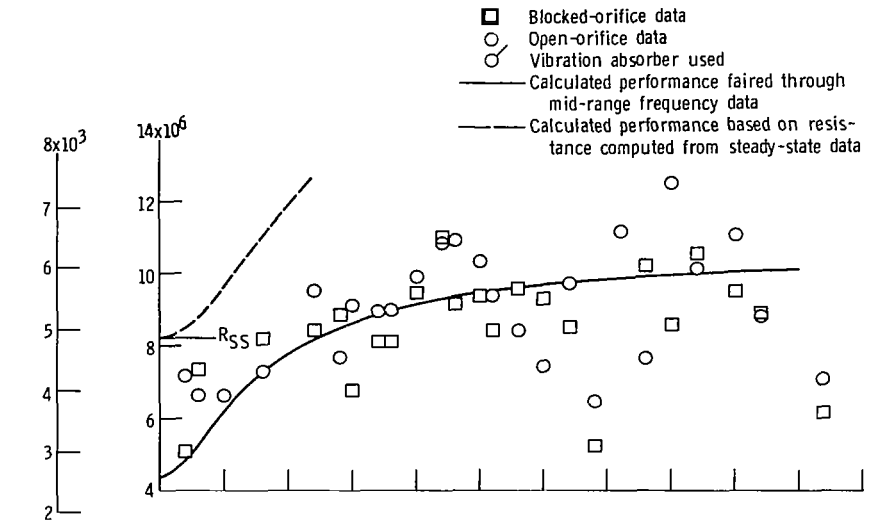

(a-1) Flow coefficient, 0.536.

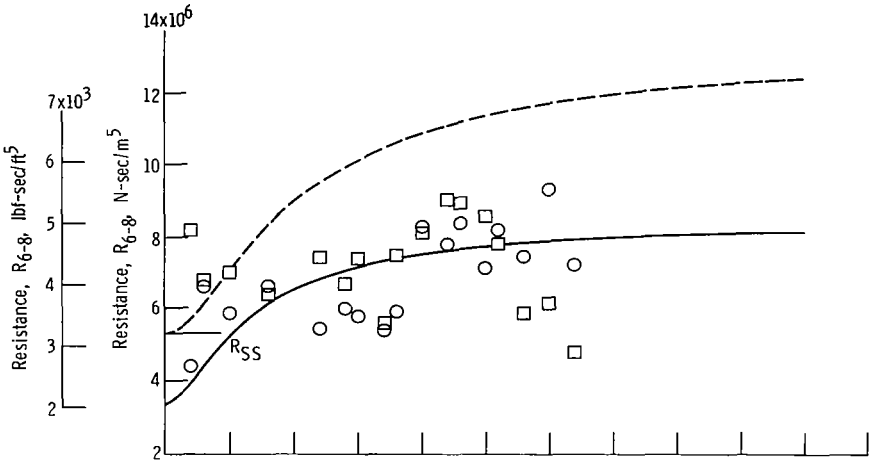

(a-2) Flow coefficient, 0.497.

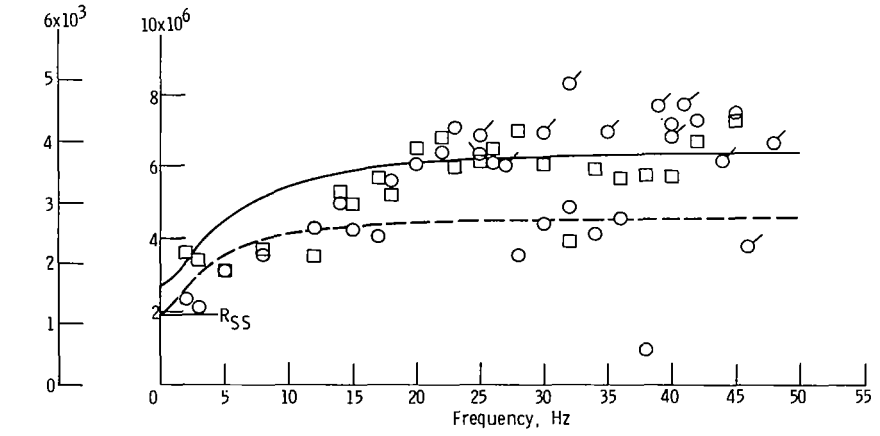

(a-3) Flow coefficient, 0.442.

(a) Resistance, R_{6-8}.

Figure 9. - Resistance and inertance across impeller and volute.

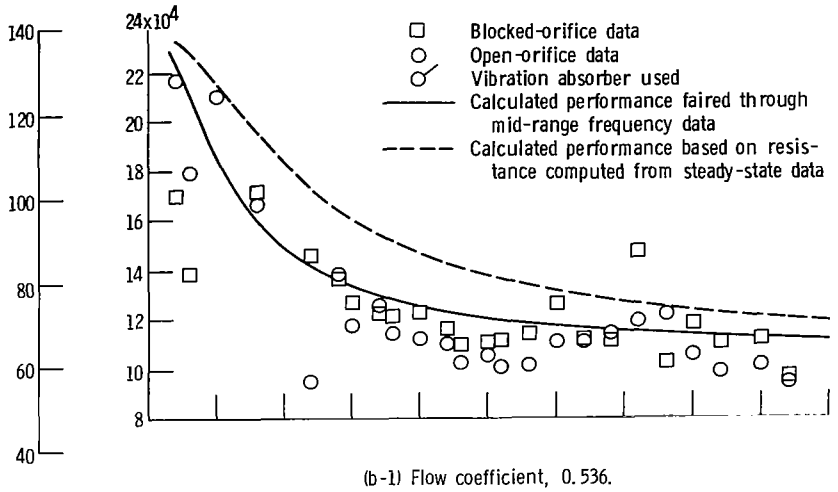

(b-1) Flow coefficient, 0.536.

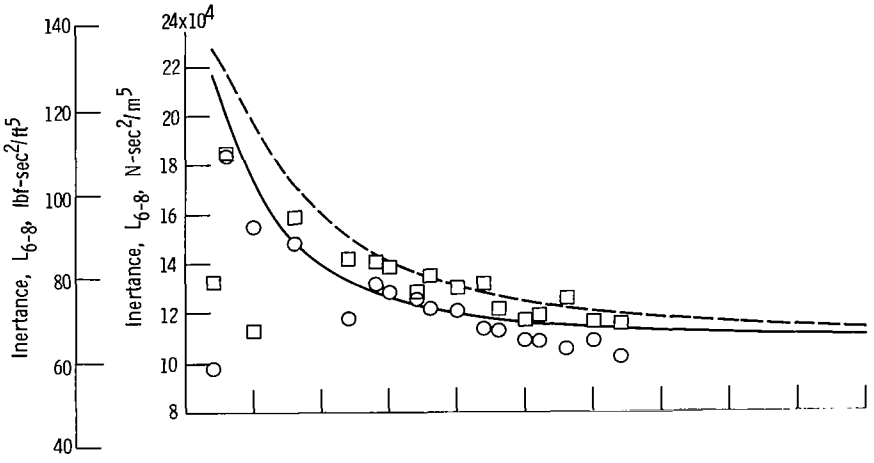

(b-2) Flow coefficient, 0.497.

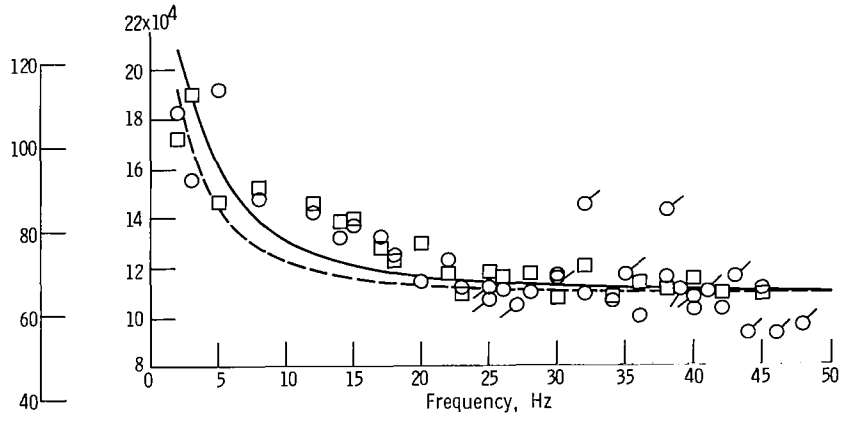

(b-3) Flow coefficient, 0.442.

(b) Pump inertance, L_{6-8}.

Figure 9. - Concluded.

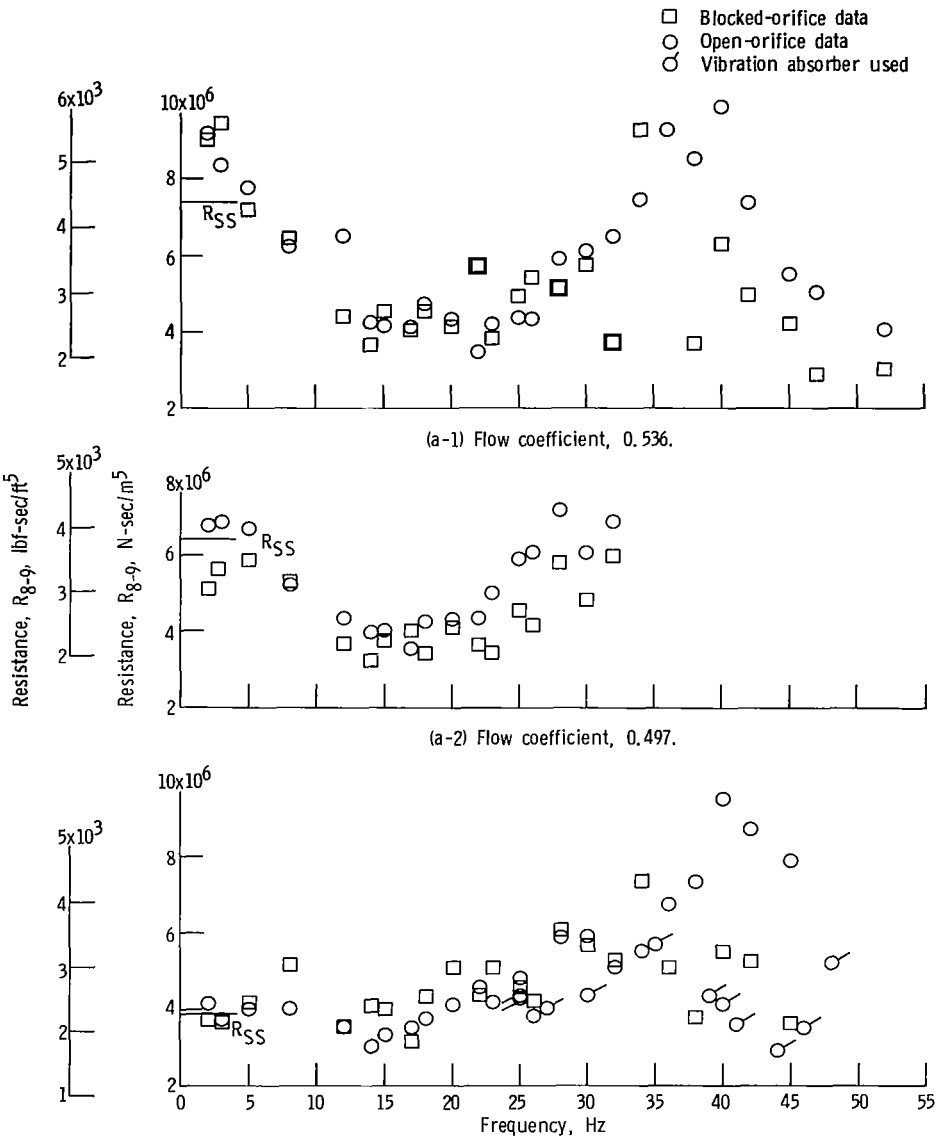

(a-1) Flow coefficient, 0.536.

(a-2) Flow coefficient, 0.497.

(a-3) Flow coefficient, 0.442.

(a) Resistance, R_{8-9}.

Figure 10. - Resistance and inertance across conical diffuser.

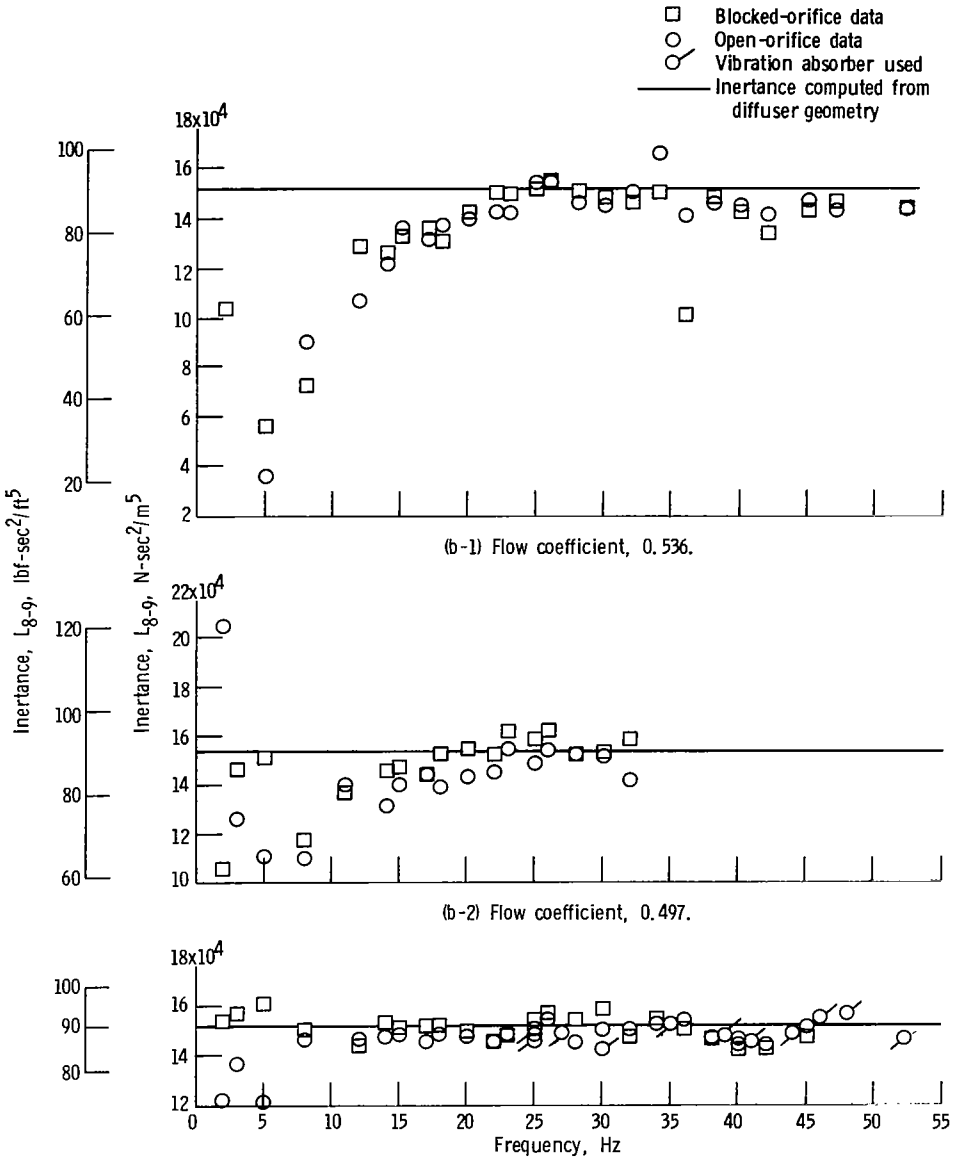

(b-1) Flow coefficient, 0.536.

(b-2) Flow coefficient, 0.497.

(b-3) Flow coefficient, 0.442.

(b) Inertance, L_{8-9}.

Figure 10. - Concluded.

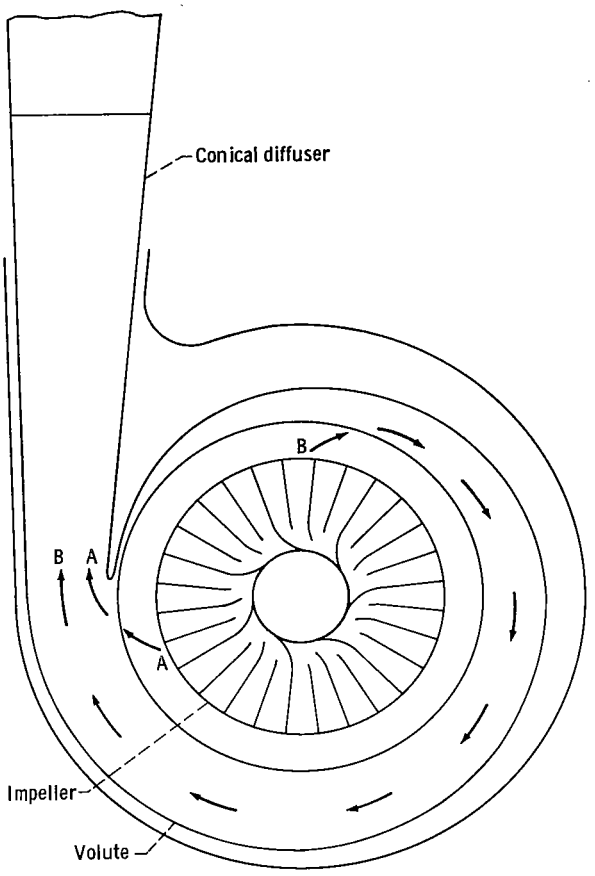

Figure 11. - Pump geometry.

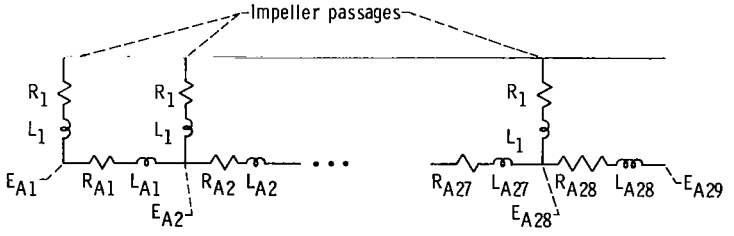

Figure 12. - Electric circuit model of pump performance.

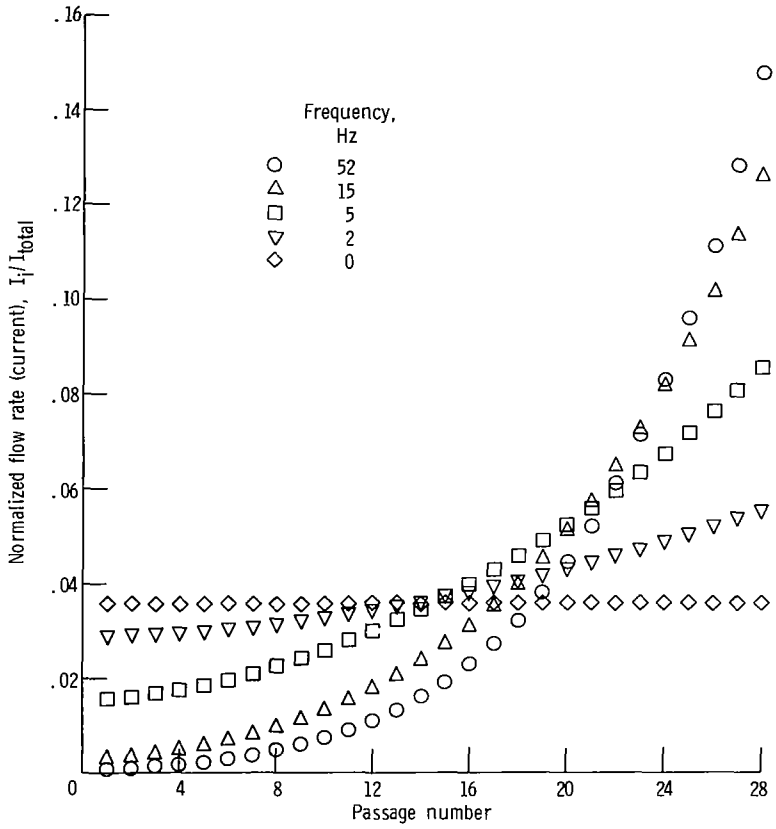

Figure 13. - Flow distribution in pump passages as computed from electric circuit model.

	R_1 and R_{A1} values, N-sec/m^5 (lbf-sec/ft^5)		
	First estimate	Reduced R_{Ai}	Zero R_{Ai}
Resistance of first section of volute, R_{A1}	5.144x10^6 (3042)	2.697x10^6 (1595)	0 (0)
Impeller passage resistance, R_1	69.33x10^6 (41 000)	72.83x10^6 (43 070)	76.63x10^6 (45 320)

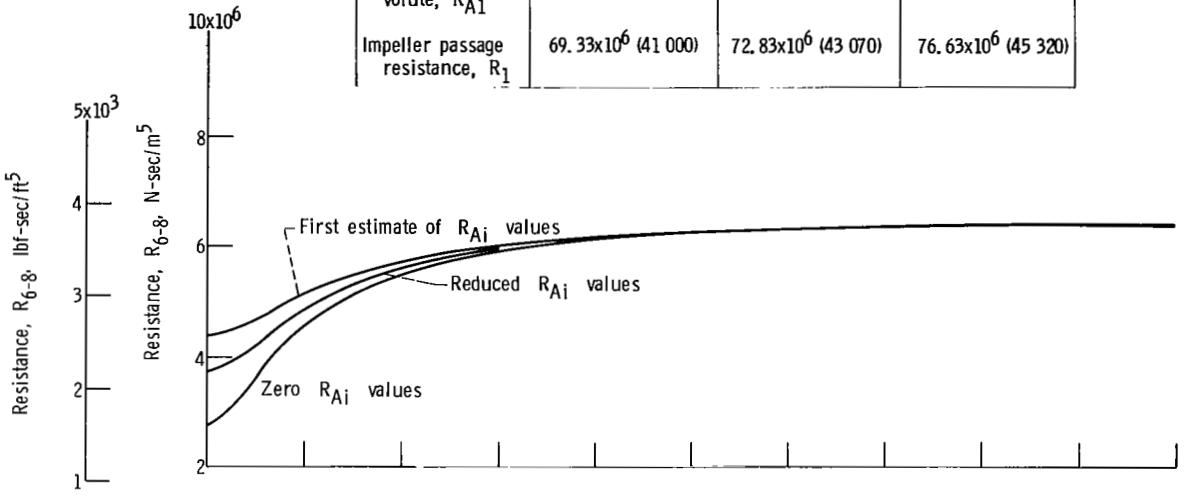

(a) Resistance, R_{6-8}.

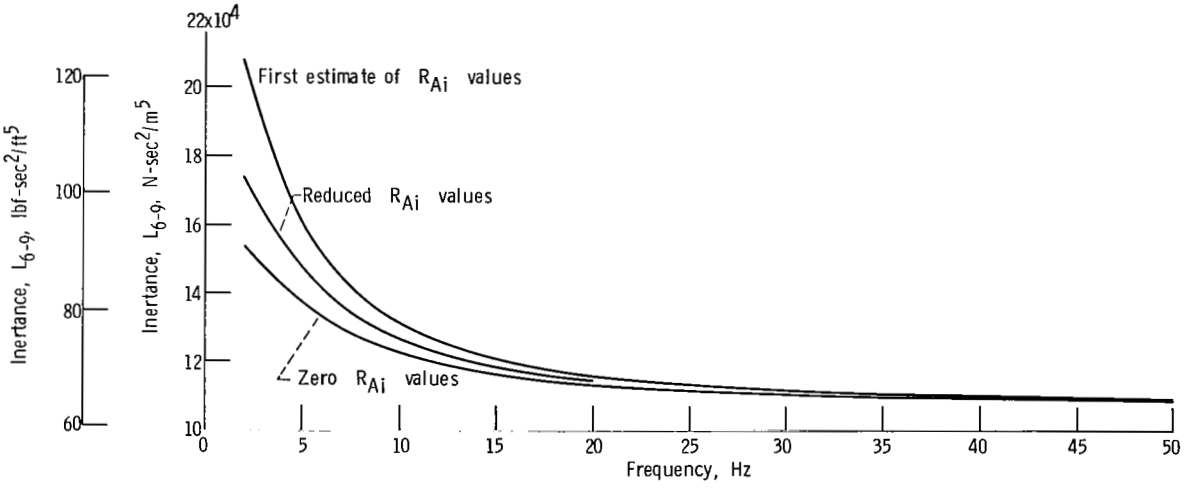

(b) Inertance, L_{6-9}.

Figure 14. - Computed resistance and inertance across impeller and volute for different relative sizes of volute resistance to impeller resistance.

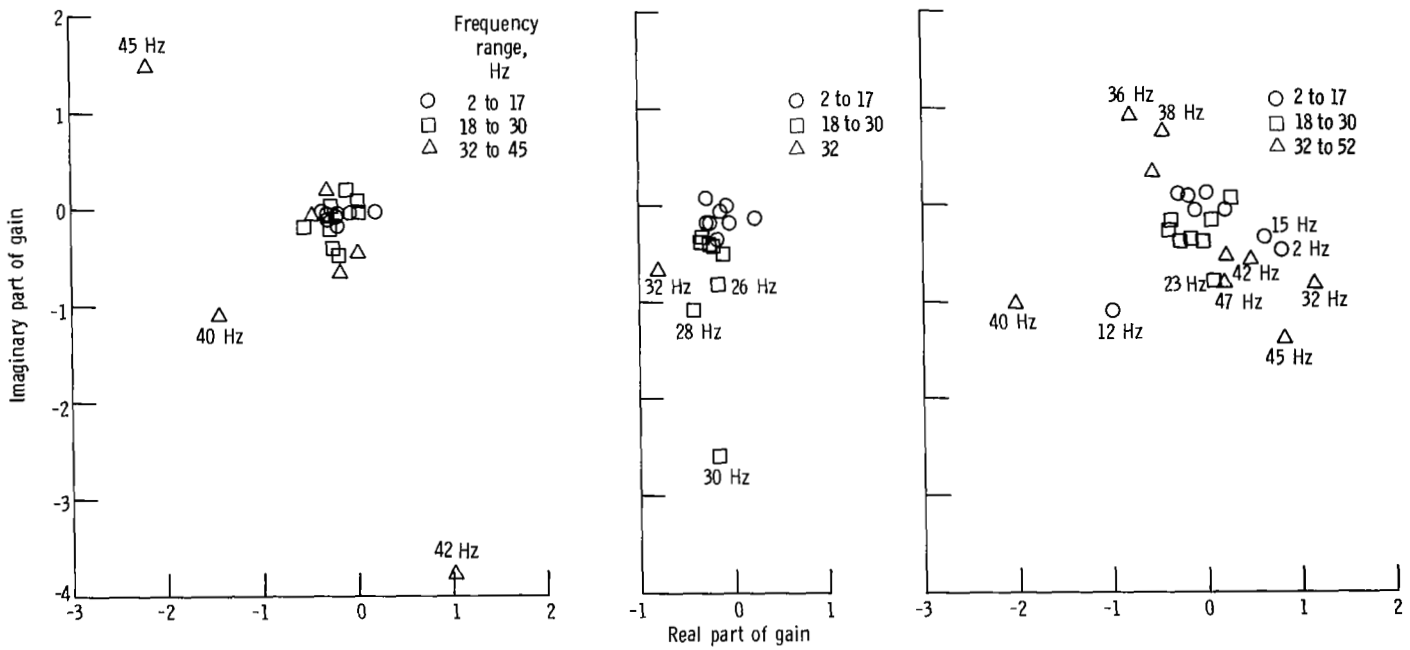

(a) Flow coefficient, 0.442.

(b) Flow coefficient, 0.497.

(c) Flow coefficient, 0.536.

Figure 15. - Pump gain.

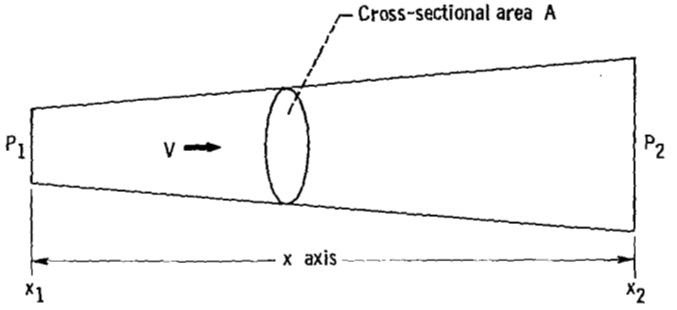

Figure 16. - One-dimensional flow.

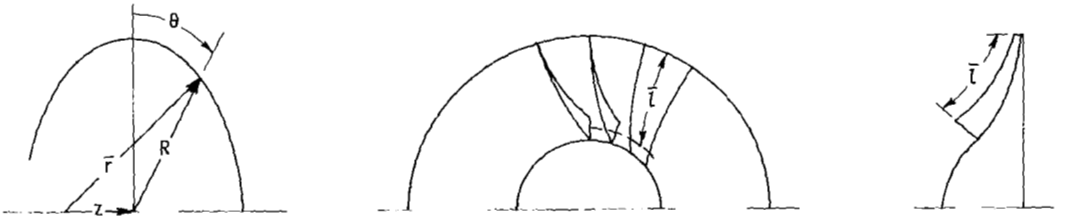

Figure 17. - Pump passage geometry.